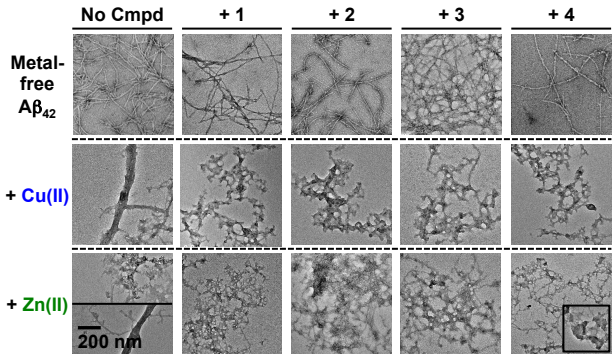

Figure 3.6. Ability of **1**-**4** to change the morphology of $A\beta_{40}$ in inhibition experiments. Images were obtained by TEM (scale bar = 200 nm).

were employed (Figure 3.7b). TEM revealed the presence of less structured forms of aggregates (Figures 3.4d, 3.5c,e, and 3.6). Similarly, **2** was also exclusively capable of managing Cu(II)–Aβ aggregation with it being more apparent for $A\beta_{42}$ (Figures 3.4b-d, 3.5b-e, and 3.6). Compound **3** was found to only have activity at higher Cu(II) concentrations (Figures 3.4b,c, 3.5b,d, and 3.7) and TEM images at 1 equiv of Cu(II) showed species with similar morphologies in comparison to the compound-untreated samples (Figures 3.4b,d, 3.5c,e, and 3.6). The Cu(II) specific activity of **1**-**3** is starkly

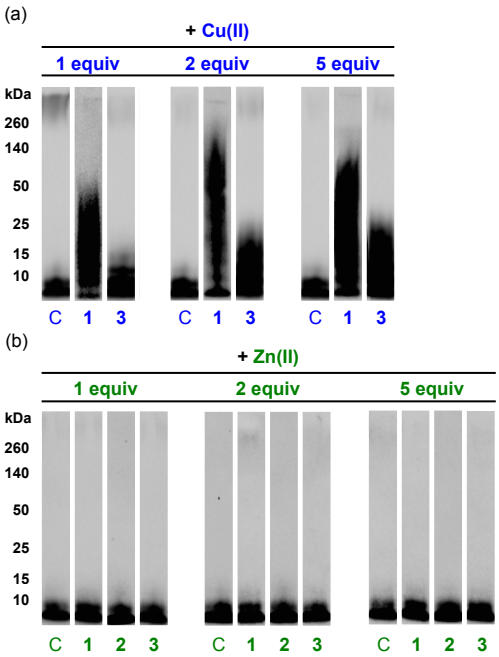

Figure 3.7. Inhibitory activity of compounds at higher metal ion concentrations on $A\beta_{40}$ aggregation (inhibition experiment). The ability of compounds to modulate the aggregation pathway of $A\beta_{40}$ in the presence of 1 equiv (left, 50 μM), 2 equiv (middle, 100 μM), and 5 equiv (right, 200 μM) of (a) Cu(II) or (b) Zn(II) was studied by gel/Western blots with an anti-Aβ antibody (6E10).

contrasted to **4** which demonstrated the ability to modulate Aβ aggregation involved by both Cu(II) and Zn(II) (Figures 3.4b,c and 3.5b,d). TEM experiments revealed the production of smaller less structured fibrils (Figures 3.4d, 3.5c,e, and 3.6). Overall, gel/Western blots and TEM investigations demonstrate that by making small changes to one framework (**1**-**4**) the ability to interact with metal-free Aβ and/or metal–Aβ and reroute the aggregation pathway to form potentially nontoxic off-pathway species[32] can be directed.

3.2.3. Reactivity II: Mediation of oxidative stress by 1-4

In addition to modulating Aβ aggregation, the potential of **1**-**4** to mediate oxidative stress was also studied. The ability of **1**-**4** to scavenge free radicals was first explored using the Trolox Equivalence Antioxidant Capacity (TEAC) assay (Figure 3.8a). This

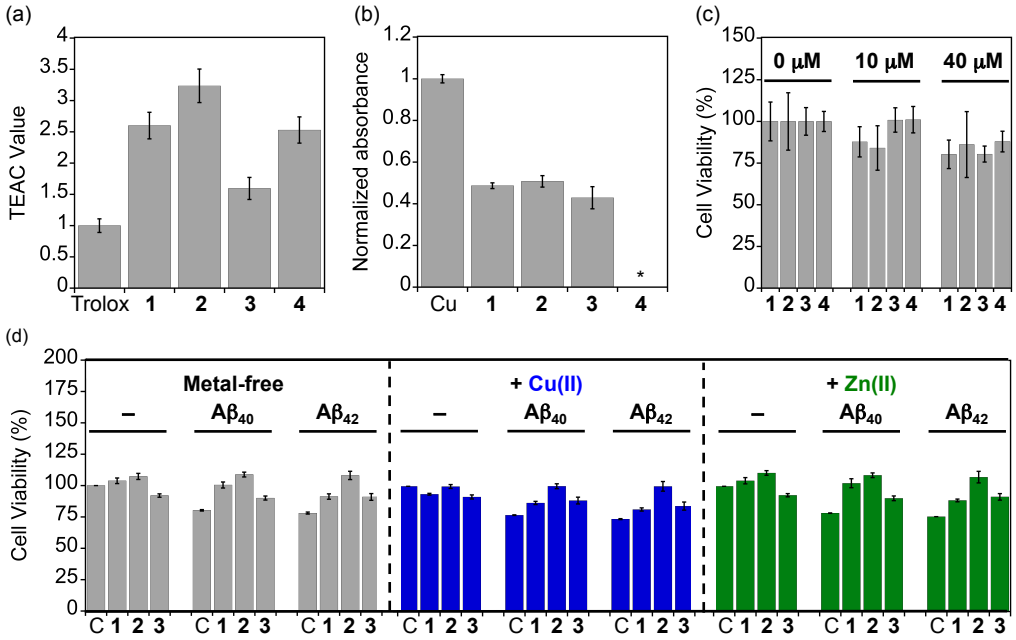

Figure 3.8. Biological activities of **1**-**4**. (a) Antioxidant activity of **1**-**4** in the presence of cell lysates as evaluated by the Trolox equivalent antioxidant capacity (TEAC) assay. All values relative to vitamin E analog **Trolox**, 6-hydroxy-2,5,7,8-tetramethylchroman-2-carboxylic acid. (b) Inhibition of Cu(I/II)–triggered Fenton-like ROS production by 1-3 (125 μM) as measured by the 2-deoxyribose assay ([Cu(II)] = 10 μM). *__4__ was not tested due to limited solubility in the assay buffer. (c) The toxicity of **1**-**4** as assessed in fetal mouse neuron cultures in the absence of metals. (d) The toxicity of **1**-**4** (20 μM) and the ability to mediate cytotoxicity of $A\beta_{40}$ (20 μM) and $A\beta_{42}$ (20 μM) in the absence (left, gray) and presence of $CuCl_2$ (middle, blue; 20 μM) or $ZnCl_2$ (right, green; 20 μM) was studied with M17 cells. C : samples without compounds. Viability of cells (%) was calculated relative to that of cells incubated only with 1% v/v DMSO. Error bars represent the standard deviation from three independent experiments. Note that **4** was not studied with Aβ species due to its noticeable toxicity with Cu(II) in the absence of the peptides.

assay was carried out in cell lysates to test the aptness of **1**-**4** to quench the organic cationic radical of 2,2'-azino-bis(3-ethylbenzothiazoline-6-sulfonic acid (ABTS) in a complex biological environment compared to known antioxidant Trolox, a water soluble analog of vitamin E.[2,33] The compounds with an functionality of amine or its derivatives (**1**, **2**, and **4**) showed a greater antioxidant capacity than Trolox, specifically, showing that **2** containing the morpholino substitution has a slightly greater capacity (*ca*. 3.2) than **1** and **4** with the amino and dimethylamino moiety, respectively (*ca.* 2.5; Figure 3.8a). In the case of **3**, the framework with two dimethoxy groups displayed its antioxidant capacity only slightly higher than Trolox (*ca.* 1.5) suggesting that an electron donating *p*-amine functionality on the backbone of small molecules can increase their antioxidant abilities (Figure 3.8a).

Additionally, the inhibitory activity of **1**-**4** toward generation of ROS by Cu(I/II) through Fenton-like reactions was evaluated using the 2-deoxyribose assay.[34] Compounds **1**-**3** were able to reduce the production of hydroxyl radicals (•OH) by approximately half (Figure 3.8b; note that **4** was not able to be tested due to poor solubility under the assay conditions). Together, both studies indicate that our frameworks with different aniline substitutions can diminish the presence and production of ROS, which could prevent oxidative stress.

3.2.4. Reactivity III: Regulation of metal-free and metal-treated peptide toxicity by 1-4

The cytotoxicity of the compounds and their ability to alleviate metal– and metal-free Aβ toxicity was explored. First, cytotoxicity was assessed employing fetal mouse neurons (Figure 3.8c) and human neuroblastoma SK-N-BE(2)-M17 (M17) cells (Figure 3.8d). In the fetal mouse neuron cultures, the compounds did not display significant toxicity in the absence of metal ions. Similar results were observed in the M17 cells where a concentration of 20 μM of **1**-**3** demonstrated to be nontoxic including when in the presence of 20 μM Cu(II) and Zn(II) with **2** having a slight trophic effect in all conditions (Figure 3.8d). **4**, however, was found to decrease cell viability in the presence of Cu(II) (*ca*. 70% viability). Additionally, when **1**-**3** was co-incubated with amyloidogenic peptides (both $A\beta_{40}$ and $A\beta_{42}$) in the absence

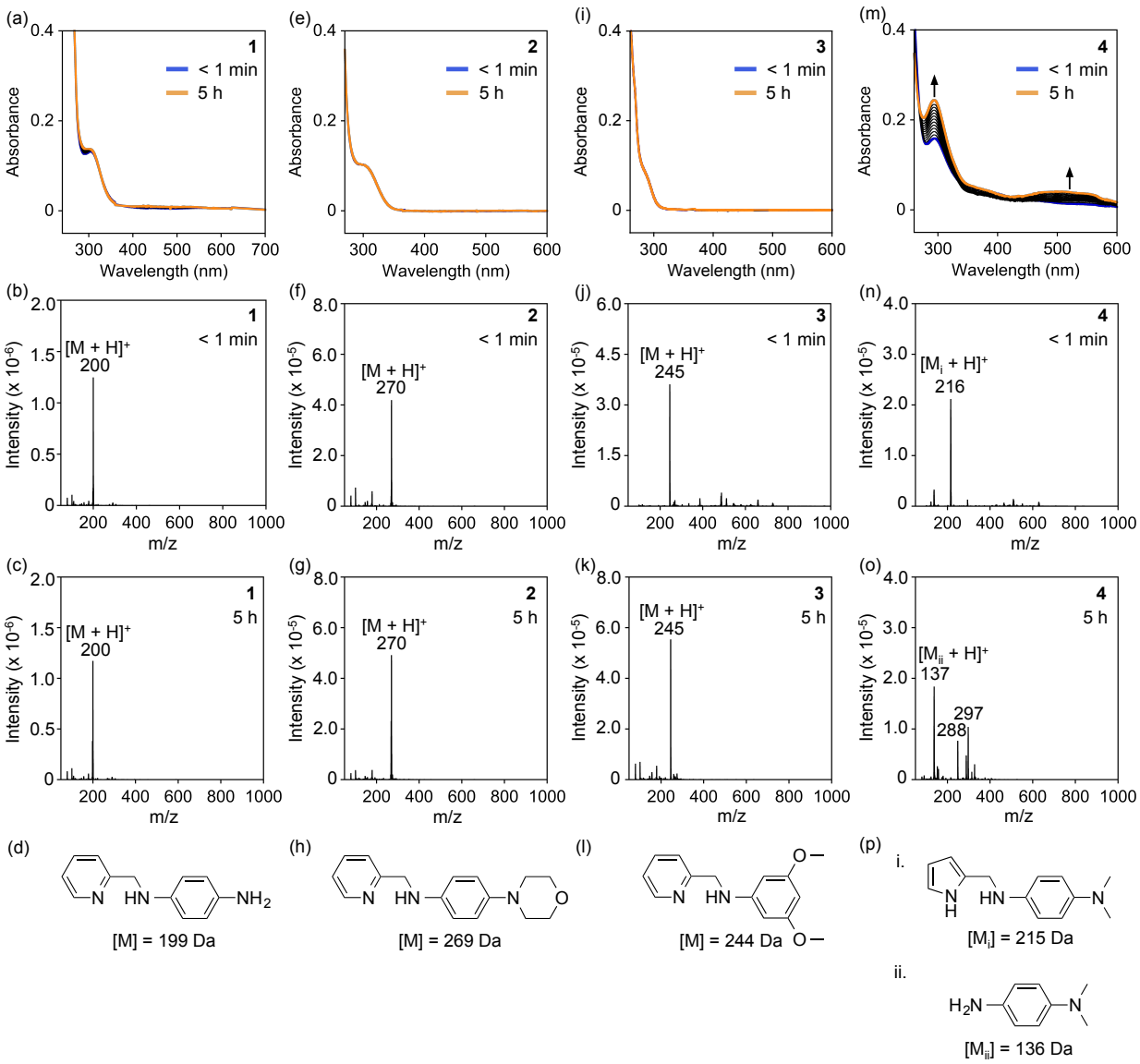

Figure 3.9. Stability studies of **1**-**4** in metal-free conditions by UV-Vis and ESI(+)MS. The stability of **1**-**4** (50 μM) by (a, e, i, m) UV-Vis in 20 μM HEPES, 150 μM NaCl, pH 7.4 over 5 h (blue: immediately after addition of sample; orange: after 5 h incubation at 37 °C) and by ESI(+)MS (b, f, j, n) immediately after addition of sample and (c, g, k, o) after incubation at 37 °C for 5 h in ddH_2O. (d, h, l, p) Structures and masses of molecules observed in the ESI(+)MS studies.

(Figure 3.8d, left) and presence of Cu(II) (Figure 3.8d, middle) and Zn(II) (Figure 3.8d, right), the toxicity induced by metal–Aβ was mediated in living cells. Noticeably, the morpholino-containing derivative (**2**) is able to completely alleviate cytotoxicity triggered by metal–Aβ.

3.2.5. Mechanistic studies I: Solution species in the absence and presence of Cu(II)

Table 3.2. Rate of transformation and half-lives of **1**-**4** in the presence and absence of Cu(II).

	Metal-free		+ Cu(II)	
Compound	***k* (abs/m)**[a]	**$t_{1/2}$ (m)**[b]	***k* (abs/m)**[a]	**$t_{1/2}$ (m)**[b]
1	–[c]	> 300	0.09 ± 0.03	7 ± 3
2	–[c]	> 300	0.04 ± 0.01	18 ± 5
3	–[c]	> 300	–[c]	> 300
4	0.016 ±0.004	44 ± 2	–[d]	< 1

[a] Rate of decay of the absorbance peak at 250, 384, and 400 nm for **4**, Cu(II) + **1**, and Cu(II) + **2**, respectfully. [b] Half life of the absorbance peak in minutes. [c] Spectra did not change during the duration of the experiment. [d] Decay of compound occurred too rapidly to measure in the experiment conditions ([**1-4**] = 50 μM, [Cu] = 25 μM, 25 μM HEPES, 150 μM NaCl, pH 7.4).

The species present in solution were first studied using UV-Vis variable-pH titrations. Changing the aniline substitutions in **1**-**3** only had a slight effect on the protonation state at physiological pH (*e.g.*, 7.4) with the predominate species in solution being the neutral form (Figure 3.9). Compounds **1**-**3** were confirmed to be stable over the tested time period of five hours (Figure 3.9a-l). Note that the pH titrations with **4** reveal that the ligand is unstable in solution. The stability of **4** was explored further by monitoring UV-Vis spectra in HEPES buffer (pH 7.4) over the course of five hours (Figure 3.9m). **4** was found to be unstable with a half life of *ca.* 40 min (Table 3.2). ESI(+)MS identified one of the breakdown products as *N*,*N*-dimethyl-*p*-phenylenediamine (**DMPD**)[35] but other possible degradation products of **4** could not be identified (Figure 3.9o,p). This could be due to the reported propensity of the pyrrole moiety to polymerize as possibly evidenced by unidentified peaks at 288 and 297 m/z (Figure 3.9o,p).[36,37] **DMPD** has been previously reported to be able to interact with and adjust both Aβ and metal–Aβ aggregation resulting in the formation of off-pathway aggregates which are non-toxic.[35]

The stability in the presence of Cu(II) was also determined (Figure 3.10). UV-Vis and ESI(+)MS studies showed that **1** and **2** both initially form CuL_2 complexes (L = ligand), with the half life of the metal complexes being *ca.* 5 min and 20 min, respectively, followed by the generation of one or two electron oxidation products (Figure 3.10a-i and Table 3.2). These types of oxidation products are well defined in the literature for unsubstituted and substituted *p*-phenylenediamine derivatives in the presence of an oxidant.[38-46] In the case of **3**, the addition of Cu(II) created a new peak at *ca.* 375 nm that did not dissipate over the five hour experiment (Figure 3.10j). ESI(+)MS

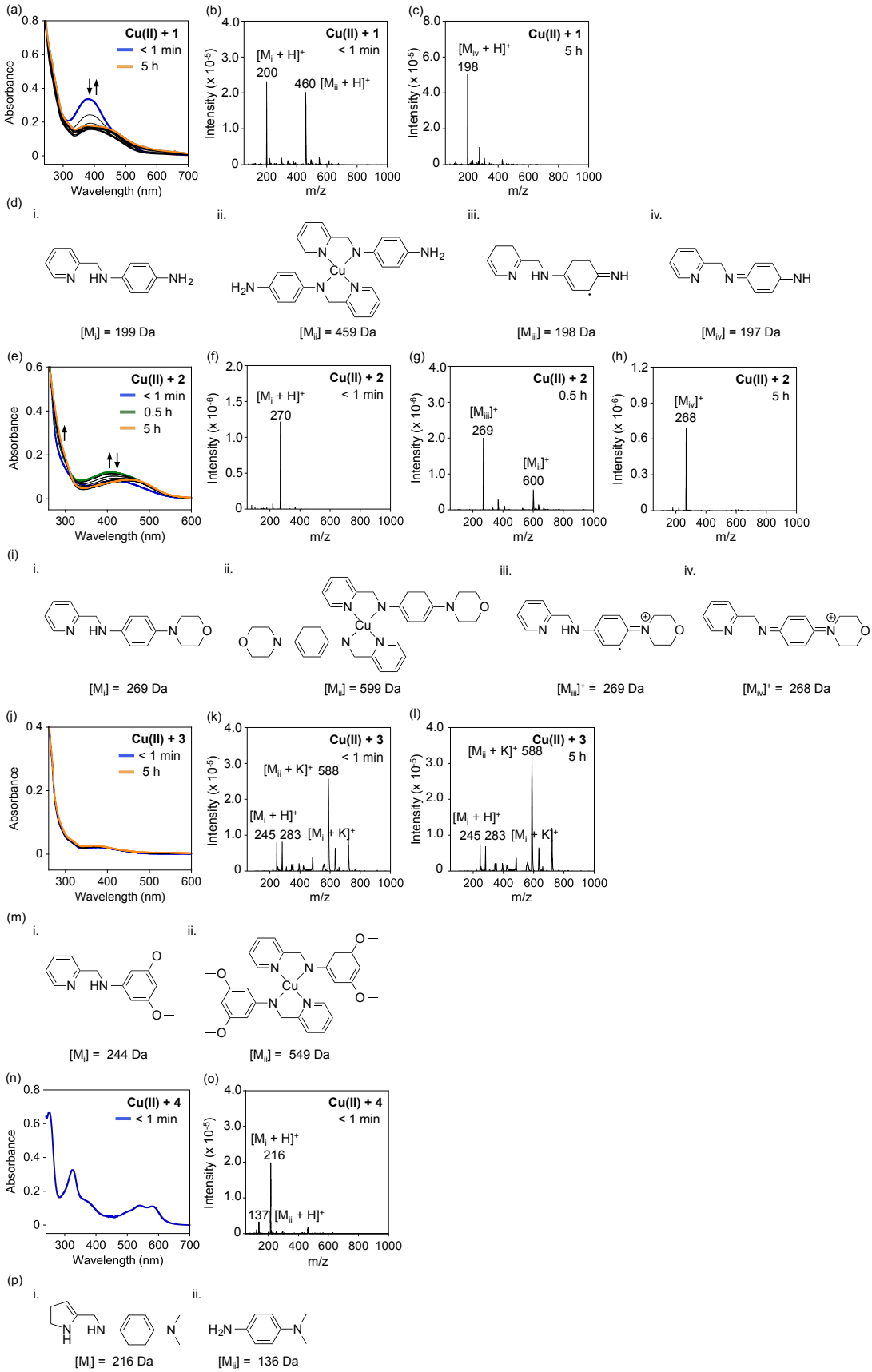
(a)
Cu(II) + 1
< 1 min
5 h
Absorbance
Wavelength (nm)
(b)
Cu(II) + 1
< 1 min
[M_i + H]+
200
460 [M_ii + H]+
Intensity (x 10-5)
m/z
(c)
Cu(II) + 1
5 h
[M_iv + H]+
198
Intensity (x 10-5)
m/z
(d)
i.
ii.
iii.
iv.
[M_i] = 199 Da
[M_ii] = 459 Da
[M_iii] = 198 Da
[M_iv] = 197 Da
(e)
Cu(II) + 2
< 1 min
0.5 h
5 h
Absorbance
Wavelength (nm)
(f)
Cu(II) + 2
< 1 min
[M_i + H]+
270
Intensity (x 10-6)
m/z
(g)
Cu(II) + 2
0.5 h
[M_iii]+
269
[M_ii]+
600
Intensity (x 10-6)
m/z
(h)
Cu(II) + 2
5 h
[M_iv]+
268
Intensity (x 10-6)
m/z
(i)
i.
ii.
iii.
iv.
[M_i] = 269 Da
[M_ii] = 599 Da
[M_iii]+ = 269 Da
[M_iv]+ = 268 Da
(j)
Cu(II) + 3
< 1 min
5 h
Absorbance
Wavelength (nm)
(k)
Cu(II) + 3
< 1 min
[M_ii + K]+ 588
[M_i + H]+
245 283 [M_i + K]+
Intensity (x 10-5)
m/z
(l)
Cu(II) + 3
5 h
[M_ii + K]+ 588
[M_i + H]+
245 283 [M_i + K]+
Intensity (x 10-5)
m/z
(m)
i.
ii.
[M_i] = 244 Da
[M_ii] = 549 Da
(n)
Cu(II) + 4
< 1 min
Absorbance
Wavelength (nm)
(o)
Cu(II) + 4
< 1 min
[M_i + H]+
216
137 [M_ii + H]+
Intensity (x 10-5)
m/z
(p)
i.
ii.
[M_i] = 216 Da
[M_ii] = 136 Da

Figure 3.10. Stability studies of **1**-**4** in the presence of Cu(II) by UV-Vis and ESI(+)MS. The stability of **1**-**4** (50 μM) in the presence of Cu(II) (25 μM) by (a, e, j, n) UV-Vis in 20 μM HEPES, 150 μM NaCl, pH 7.4 over 5 h (blue: immediately after addition of sample; green: after 0.5 h incubation; orange: after 5 h incubation at 37 °C) and by ESI(+)MS (b, f, k, o) immediately after addition of sample and after incubation at 37 °C for (g) 0.5 h, and (c, h, l) 5 h in ddH_2O. (d, i, m, p) Structures and masses of molecules observed in the ESI(+)MS studies.

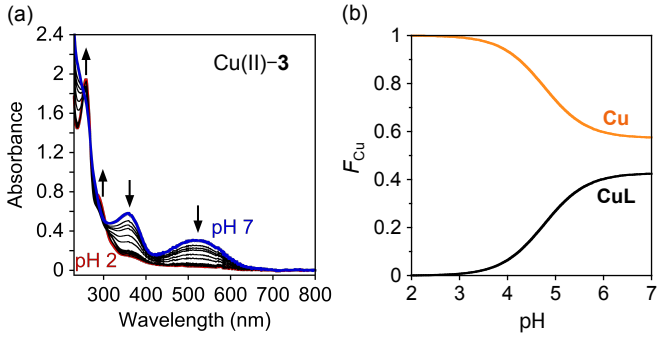

(c)

			logβ
		L =	**3**
Cu	+ **L**	**CuL**	5.6(8)
pCu (=–log[Cu(II)]$_{free}$; pH 6.6)			6.24

Figure 3.11. Solution speciation studies of Cu(II)–**3** complexes. UV-Vis titration spectra for (a) Cu(II)–**3** were fit to determine (c) stability constants (logβ) of Cu(II)–L species and (b) used to generate speciation diagrams (F_{Cu} = Fraction of free Cu and Cu(II)–L). Parenthesis indicate that the error is in the last digit of the values. Conditions: Cu(II):L = 1:2, [**3**] = 50 μM; samples were incubated at room temperature for 24 h before titrations. Charges omitted for clarity.

identified this as the CuL_2 complex (Figure 3.10k-m). Different from **1** and **2**, **3** forms a complex with Cu(II) without any further transformations; thus, the binding affinity (K_d) of **3** for Cu(II) was estimated using UV-Vis variable-pH titrations were carried out on a solution of Cu(II) and **3** (Cu(II):**3** = 1:2; 100 mM NaCl, 10 mM NaOH; Figure 3.11). These experiments indicated the presence of a 1:1 complex under the experimental conditions with a stability constant (logβ) of 5.6(8). Based on this value and the pK_a values of **3**, a speciation diagram was modeled and the pCu (pCu = –log[$Cu_{unchelated}$]) was calculated to be 6.24 suggesting an approximate disassociation constant in the micromolar range (Figure 3.11b, $K_d \approx$ [$Cu_{unchelated}$]). This low binding affinity is most likely too weak to interact with the low micromolar to high picomolar (*ca.* 10^{-7} – 10^{-11} M) binding affinity for the first Cu(II) binding site of Aβ. Interaction is possible, however, with the second metal binding site which has a weaker affinity of *ca.* 10^{-5} M for Cu(II).[2,47,48] This is consistent with the gel/Western blot experiments where at least two equivalents

of Cu(II) required before activity can be observed suggesting **3** can only interact with Aβ when both metal binding sites are metalated (*vide supra*).

Additionally, the absorption bands at 360 nm and 530 nm from the Cu(II)-**3** complex were assigned using the concentration of this complex as determined from the speciation diagram and the Beer-Lambert law.[49] The molar absorption coefficient (ε) for these bands was estimated to be *ca*. 20,100 $M^{-1}cm^{-1}$ and 12,700 $M^{-1}cm^{-1}$ for the bands at 360 and 530 nm, respectively. These values suggest that both absorptions are not from d-d transitions and most likely arise from charge transfer properties.

Addition of Cu(II) to **4** resulted in intense double peaked optical bands at *ca.* 510 and 550 nm, which is similar to the previously reported spectra of the cationic radical of **DMPD** (Figure 3.10n).[35] The identity of this species, however, is unclear with ESI(+)MS taken immediately after the start of the experiment showing peaks at *m*/*z* 138 and 215 within error of **DMPD** and **4** or their oxidized forms (Figure 3.10o,p); note that longer incubations lead to the precipitation of the sample limiting analysis of the species in solution). This suggests that like in the case of metal-free Aβ (*vide supra*) that **DMPD** is responsible for the activity observed.[35]

3.2.6. Mechanistic studies III: Computational studies

To further elucidate the mode of action of **1**-**4** toward Aβ in the presence of Cu(II), DFT calculations were employed. First, calculations of the activation energy for the hydrolysis of C–N bond assisted by Cu(II) were carried out (Figure 3.12a-c,f). Only the S_N2-type hydrolysis was considered due to the decreased complexity of modeling the transition state of this mecanism compared to S_N1. In this mechanism, Cu(II) coordination, either in a bidentate (**1**-**3**) or monodentate (**4**) fashion, enhances the leaving group ability of the arylamine moiety. **4** was found to have a low barrier for hydrolysis compared to **1**-**3** (Figure 3.12f). This can be attributed to the ability of electron-rich pyrrole moiety to stabilize the transition state, and to the inability of the protonated pyrrolic nitrogen to coordinate to Cu(II) which resulted in a rather symmetric transition state due to the stabilization of the carbocation species (Figure 3.12c). The pyridine moiety in **1**-**3** cannot provide enough stabilization to the cation-like transition state, thus the water molecule was required to be closer to the nucleophilic center

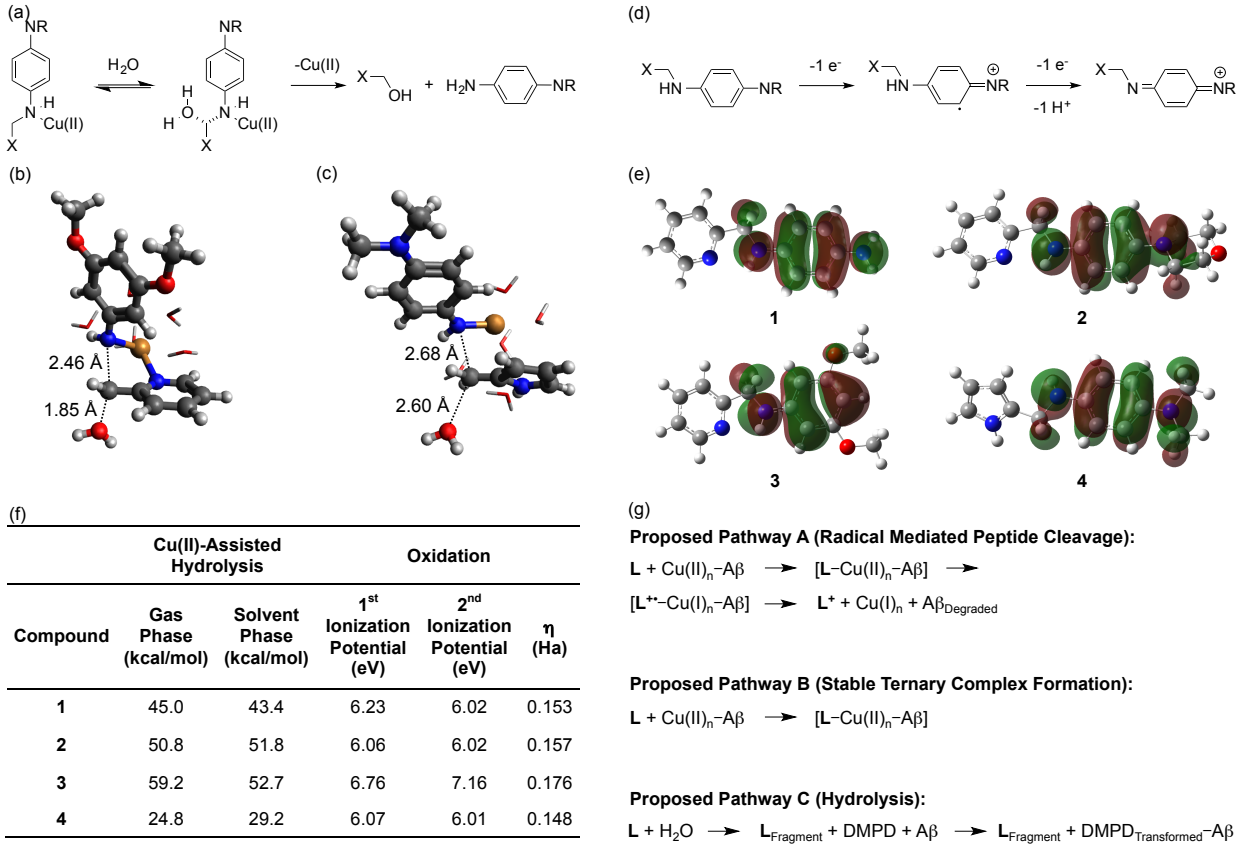

(f)

Compound	Cu(II)-Assisted Hydrolysis: Gas Phase (kcal/mol)	Cu(II)-Assisted Hydrolysis: Solvent Phase (kcal/mol)	Oxidation: 1st Ionization Potential (eV)	Oxidation: 2nd Ionization Potential (eV)	Oxidation: η (Ha)
1	45.0	43.4	6.23	6.02	0.153
2	50.8	51.8	6.06	6.02	0.157
3	59.2	52.7	6.76	7.16	0.176
4	24.8	29.2	6.07	6.01	0.148

(g)

Proposed Pathway A (Radical Mediated Peptide Cleavage):

L + $Cu(II)_n$–Aβ → [**L**–$Cu(II)_n$–Aβ] →

[$\mathbf{L}^{+\bullet}$–$Cu(I)_n$–Aβ] → $\mathbf{L}^{+}$ + $Cu(I)_n$ + $Aβ_{Degraded}$

Proposed Pathway B (Stable Ternary Complex Formation):

L + $Cu(II)_n$–Aβ → [**L**–$Cu(II)_n$–Aβ]

Proposed Pathway C (Hydrolysis):

L + H_2O → $\mathbf{L}_{Fragment}$ + DMPD + Aβ → $\mathbf{L}_{Fragment}$ + $DMPD_{Transformed}$–Aβ

Figure 3.12. Computational investigations of the molecular level properties of **1**-**4** and proposed mechanistic pathways. (a) Scheme of the S_N2 Cu(II)-assisted hydrolysis of **1**-**4** and the DFT optimized transition state structures of the hydrolysis of (b) **3** and (c) **4**. The bond lengths of bonds being broken and being formed are shown. For clarity, the water molecules coordinating to Cu(II) are represented with sticks (red: O; blue: N; gray: C; white: H; orange: Cu). (d) Scheme of oxidation of *p*-phenylenediamines. (e) Isosurface plot of SOMOs of **1**-**4** with an isovalue of 0.02 au. Red represents the electron phase while green represents the opposite phase. (f) Calculated activation energies in the gas and in solvent (water) phase as well as ionization potentials and chemical hardness (η; $\eta \approx \varepsilon_{LUMO} - \varepsilon_{HOMO}$) for **1**-**4**. (g) Proposed pathways for the differing activities of **1**-**4** toward metal-free or metal-associated Aβ species.

(Figure 3.12b,c). Furthermore, the requirement that both nitrogen atoms of **1**-**3** should be coordinating to Cu(II) leads to a distortion around the arylamine nitrogen atom which is not present for **4** (Figure 3.12b,c). These calculations suggest that **4** was more likely than **1**-**3** to undergo hydrolysis to produce **DMPD**, which is in agreement with the UV-Vis and ESI(+)MS studies (*vide supra*).

The one and two electron ionization potentials for **1**-**4** were also calculated (Figure 3.13d,f). Furthermore, the chemical hardness (η), $\eta \approx \varepsilon_{LUMO} - \varepsilon_{HOMO}$ where ε_{LUMO} and ε_{HOMO} are energies of lowest unoccupied molecular orbital (LUMO) and highest occupied molecular orbital (HOMO) orbitals, respectively, was used as an electronic structure parameter for measuring oxidation tendency (Figure 3.12f). These studies

show that **3** has higher one and two electron ionization potentials compared to **1, 2**, and **4**. This is because the unpaired electron in cation radical species is mainly stabilized *via* π-delocalization on the benzene ring, σ-conjugation on *para*-substituted position, and combinations of π-delocalization and σ-conjugation features. As shown in Figure 3.12e, the singly occupied molecular orbitals (SOMOs) of the cationic radicals of **1, 2**, and **4** are located on the benzene ring and the *para*-diamino substitution (*via* π-delocalization and σ-conjugation features) whereas the radical on **3** is mainly located at the benzene ring. Additionally, the *para*-substituted groups of **1, 2**, and **4** are mixed into the SOMO, but *meta*-substitutions in **3** do not. Therefore, the amino groups in **1, 2**, and **4** raises the SOMOs level by its mesomeric effect, in contrast to the methoxy groups in **3** can only act as an inductive withdrawer to lower the SOMOs. As a result, **3** was characterized by higher value of chemical hardness than the others implying a lower tendency to undergo oxidation.

3.2.7. Proposed modes of action of 1-4 toward metal-free and metal-peptide reactivity

Collecting the results from our investigations, we propose the multiple modes of action in our systems employing **1**-**4**. First, the mode of action of mediating the aggregation of Aβ and metal–Aβ is proposed. Studies presented here and previous studies with structurally similar compounds[14,18] suggest that the mode of action of **1** and **2** could involve the development of a transient ternary complex between the compounds, Aβ and Cu(II). This could be subsequently followed by the one electron oxidation of **1** and **2** by Cu(II) resulting in the formation of their cationic radicals and in the presence of Aβ leads to the degradation of the peptide by well documented radical pathways (proposed pathway A, Figure 3.12g).[50-53]

In contrast to these radical mechanisms, **3**, due to the higher calculated ionization potentials most likely undergoes a different pathway of Aβ aggregation modulation. Thus, it is proposed that the interaction of **3** with Cu(II)–Aβ results in the formation of a stable ternary complex consisting of Aβ, Cu(II), and **3** which subsequently changes the species reactivity (proposed pathway B, Figure 3.12g). In the case of **4**, based on the DFT calculations which predict that hydrolysis occurs, this molecule most likely

hydrolyzes to produce **DMPD**, which is responsible for interaction and reactivity with both metal-free and metal-associated Aβ, following proposed mode of action C (Figure 3.12g).

Additionally, **1**-**4** most likely can mediate oxidative stress caused by the presence of organic radicals by acting as antioxidants to donate an electron to quench the radials.[54,55] This is evidenced by their activity toward the radicals correlating the calculated ionization potentials, which measure the ease of releasing an electron. Furthermore, in the presence of Cu(I/II), **1**-**3** can also inhibit the formation of ROS. Since their activity is similar this suggests that these compounds exert their activity mainly by binding to the Cu(I/II) and preventing H_2O_2 from coordinating to the metal and being reduced to form hydroxyl radicals.[55] The previously discussed electron donating properties of the compounds, however, could also compliment this activity. A more in depth understanding of the modes of action of **1**-**4** will be the subject of future studies.

3.3. Concluding remarks

The initial studies presented here demonstrate that minor structural variations to small molecules can completely alter their ability to modulate the interrelationship between metal ions, amyloidogenic peptides, and oxidative stress to different degrees. Investigations of these varied activities revealed a structure-reactivity-mechanism relationship. The molecular level understanding generated though these studies will allow for the ability to control the target and degree of modulation of multiple pathogenic factors of neurodegenerative diseases. This affords a level of control that will allow for the future development of molecules as both chemical tools and therapeutics that can specifically probe certain features of these devastating diseases.

3.4. Experimental section

3.4.1. Materials and methods

All reagents were purchased from commercial suppliers and used as received unless otherwise noted. $A\beta_{40}$ and $A\beta_{42}$ (the sequence of $A\beta_{42}$: DAEFRHDSGYE-VHHQKLVFFAEDVGSNKGAIIGLMVGGVVIA) were purchased from Anaspec Inc.

(Fremont, CA, USA). Trace metals were removed from buffers and solutions used in Aβ experiments by treating with Chelex overnight (Sigma-Aldrich, St. Louis, MO, USA). Optical spectra were recorded on an Agilent 8453 UV-visible (UV-Vis) spectrophotometer. Absorbance values for biological assays, including cell viability and antioxidant assays, were measured on a Molecular Devices SpectraMax 190 microplate reader (Sunnyvale, CA, USA). ^{1}H and ^{13}C 1D spectra were recorded using a 400 MHz Agilent NMR spectrometer.

3.4.2. Preparation of 4-nitro-*N*-(pyridin-2-ylmethyl)aniline

Synthesized using previously reported methods with modifications.[19] To a flame dried flask equipped with a magnetic bar and reflux condenser under N_2 atmosphere. A solution of 1-fluoro-4-nitrobenzene (231 μL, 2.2 mmol) and *N*,*N*-diisopropylethylamine (836 μL, 4.8 mmol) in DMF (25 mL) was stirred at room temperature before the addition of 2-(aminomethyl)pyridine (247 μL, 2.4 mmol). The reaction was heated to 70 °C. After 24 h, the brown solution was added to water (75 mL) and extracted with EtOAc (3 x 75 mL). The organic layers were washed with water (2 x 75 mL) and brine (75 mL). Then dried with $MgSO_4$ and concentrated under vacuum. The resulting residue was then purified by silica column chromatography (25% to 100% EtOAc in hexanes) yielding a yellow solid (288 mg, 58%). TLC (EtOAc:hexanes, 50:50 v/v). R_f = 0.25; ^{1}H NMR (400 MHz, CD_2Cl_2): δ 8.56 (d, 1H, *J* = 8 Hz), 8.09 (d, 2H, *J* = 8 Hz), 7.71 (t, 1H, *J* = 8 Hz), 7.30 (d, 1H, *J* = 8 Hz), 7.25 (d, 1H, *J* = 4 Hz), 6.68 (d, 2 H, *J* = 8 Hz), 6.04 (s, 1H), 4.53 (d, 2H, *J* = 8 Hz). ^{13}C NMR (100 MHz CD_2Cl_2): δ 156.2, 153.5, 149.5, 138.5, 137.2, 126.6, 123.0, 122.1, 111.8, 48.2.

3.4.3. Preparation of 1

Purchased from Ryan Scientific (Mt. Pleasant, SC, USA) and recrystallized from dichloromethane/hexanes four times. Tan powder ^{1}H NMR [400 MHz $(CD_3)_2SO$]: δ 8.49 (d, 1H, *J* = 4 Hz), 7.70 (t, 1H, *J* = 4 Hz), 7.35 (d, 1H, *J* = 4 Hz), 7.22 (t, 1H, *J* = 4 Hz), 6.36 (m, 4H), 5.46 (s, 1H), 4.23 (m, 4H). ^{13}C NMR (100 MHz CD_2Cl_2): δ 159.58, 149.50, 141.44, 138.65, 136.75, 122.30, 121.99, 116.85, 114.88, 50.69; ESI(+)MS (*m*/z): $[M+H]^+$ Calcd. for $C_{12}H_{14}N_3$, 200.11; found, 200.03.

Additionally, **1** was also synthesized by adapting previously reported methods[20] to reduce 4-nitro-*N*-(pyridin-2-ylmethyl)aniline. To a solution of 4-nitro-*N*-(pyridin-2-ylmethyl)aniline (518 mg, 2.26 mmol) and *tris*(acetylacetonato)iron(III) (23.9 mg, 3 mol%) in ethanol (20 mL) in a round bottom flask equipped with a stirbar and reflux condenser, hydrazine hydrate (581 μL, 11.3 μmol) was added. The solution was then heated under reflux for 2 h and 4 additional equivalents of hydrazine hydrate was added. The mixture was allowed to react for an additional 3 h before removing the solvent under vacuum. The resulting brown oil was purified by silica column chromatography [100% EtOAc to 99% EtOAc: 1% Et_3N; TLC (EtOAc:Et_3N, 99:1 v/v); R_f = 0.20]. The HCl salt of the product was then prepared by dissolving in MeOH and adding excess 5M HCl. The solvent was removed on under vacuum and the resulting residue was washed with Et_2O(3 x 5 mL) before being dissolved in water (20 mL) and washed with Et_2O (3 x 20 mL). The aqueous layer was collected and the product was obtained lyophilization (grey powder, 0.4485 g. 84.5%). ^{1}H NMR [400 MHz, $(CD_3)_2SO$]: δ 9.59 (s, 1H), 8.59 (d, 1H, *J* = 4 Hz), 7.90 (t, 1H, *J* = 4 Hz), 7.59 (m, 2H), 7.05 (d, 2H, *J* = 8 Hz), 6.67 (d, 2H, *J* = 8 Hz), 4.43 (s, 2H). ^{13}C NMR (100 MHz, $(CD_3)_2SO$): δ 156.0, 147.1, 144.6, 142.9, 125.0, 124.6, 124.0, 120.8, 113.0, 44.8.

3.4.4. Preparation of 2

Purchased from Ryan Scientific, dried under vacuum to remove all traces of solvents, and used without any farther purification (tan powder). ^{1}H NMR [400 MHz, $(CD_3)_2SO$]: δ 8.51 (d, 1H, *J* = 4 Hz), 7.71 (t, 1H, *J* = 8 Hz), 7.21 (d, 1H, *J* = 8 Hz), 7.24 (d, 1H, *J* = 8 Hz), 6.73 (d, 2H, *J* = 8 Hz), 6.51 (d, 2H, *J* = 8 Hz), 5.93 (t, 1H, *J* = 8 Hz), 4.29 (d, 2H, J = 4 Hz), 3.68 (t, 4H, *J* = 4 Hz), 2.86 (t, 4H, *J* = 4 Hz). ^{13}C NMR (100 MHz, CD_2Cl_2): δ 159.2, 149.5, 144.1, 142.8, 136.7, 122.3, 121.89, 118.4, 114.2, 67.39, 51.5, 50.2. HRMS (*m/z*): $[M+H]^+$ Calcd. for $C_{16}H_{20}N_3O$, 270.1601; found, 270.1595.

3.4.5. Preparation of 3

Purchased from Ryan Scientific and recrystallized from acetonitrile and water three times (off-white powder). ^{1}H NMR [400 MHz, $(CD_3)_2SO$]: δ 8.52 (d, 1H, *J* = 4 Hz), 7.73 (t, 1H, *J* = 8 Hz), 7.35 (d, 1H, *J* = 8 Hz), 7.24 (t, 1H, *J* = 8 Hz), 6.35 (t, 1H, *J* = 8 Hz),

5.75 (s, 2H), 5.71 (s, 1H), 4.31 (d, 2H, 4 Hz), 3.61 (s, 6H). ^{13}C NMR (100 MHz, $(CD_3)_2SO$): δ 161.1, 159.8, 150.2, 148.8, 136.6, 122.0, 121.1, 91.1, 88.6, 54.7, 48.5. HRMS (*m/z*): $[M+H]^+$ Calcd. for $C_{14}H_{17}N_2O_2$, 245.1285; found, 245.1287.

3.4.6. Preparation of 4

Purchased from Ukrorgsyntez (Ukraine), washed with hexanes with one drop of dichloromethane once and hexanes three times repeatedly (3 or 4 times) until pure by ^{1}H NMR (dark brown powder). ^{1}H NMR [400 MHz, $(CD_3)_2SO$]: δ 10.65 (s, 1H), 6.60 (m, 4H), 5.91 (s, 2H), 5.09 (s, 1H), 4.07 (d, 2H, *J* = 8 Hz), 2.70 (s, 6H). ^{13}C NMR (100 MHz, CD_2Cl_2): δ 145.3, 140.9, 130.8, 117.6, 115.9, 115.2, 108.7, 106.3, 43.20, 42.27. HRMS (*m/z*): $[M]^+$ Calcd. for $C_{13}H_{17}N_3$, 215.1417; found, 215.1415.

3.4.7. Parallel artificial membrane permeability assay adapted for blood-brain barrier (PAMPA-BBB)

PAMPA-BBB experiments were carried out using the PAMPA Explorer kit (*p*ION Inc., Billerica, MA, USA) using previously reported protocols.[56] Compounds (25 μM, 200 μL) in pH 7.4 Prisma HT buffer (*p*ION) were added to the wells of a donor plate (number of replicates = 12). The polyvinylidene fluoride (PVDF, 0.45 μM) filter membrane on the acceptor plate was coated with BBB-1 lipid formulation (5 μL, *p*ION). The acceptor plate was placed on top of the donor plate, brain sink buffer (BSB, 200 μL, *p*ION) was added to each well of the acceptor plate and was incubated for 4 h at ambient temperature without stirring. UV−Vis spectra of the solutions in the reference, acceptor, and donor plates were measured using a microplate reader. The PAMPA Explorer software v. 3.5 (*p*ION) was used to calculate the $-\log P_e$ values for the compounds. CNS± designations were assigned by comparison to compounds that were identified in previous reports.[14,57-59]

3.4.8. Aβ aggregation experiments

Aβ experiments were performed according to previously published methods.[14,18,32,33,56,60,61] Prior to experiments, $A\beta_{40}$ or $A\beta_{42}$ was dissolved in ammonium

hydroxide (NH_4OH; 1% v/v, aq). The resulting solution was aliquoted, lyophilized overnight, and stored at −80 °C. A stock solution of Aβ was then prepared by dissolving lyophilized peptide in 1% NH_4OH (10 μL) and diluting with ddH_2O. The concentration of the solution was determined by measuring the absorbance of the solution at 280 nm (ε = 1450 $M^{-1}cm^{-1}$ for $A\beta_{40}$; ε = 1490 $M^{-1}cm^{-1}$ for $A\beta_{42}$). The peptide stock solution was diluted to a final concentration of 25 μM in Chelex-treated buffered solution containing HEPES (20 μM, pH 6.6 for Cu(II) samples; pH 7.4 for metal-free and Zn(II) samples) and NaCl (150 μM). For the inhibition studies, compounds (final concentration 50 μM, 1% v/v DMSO) were added to the sample of Aβ (25 μM) in the absence and presence of a metal chloride salt ($CuCl_2$ or $ZnCl_2$; 25, 50, 100 or 125 μM) followed by incubation at 37 °C with constant agitation for 24 h. For the disaggregation studies, Aβ with and without a metal chloride salt was incubated for 24 h at 37 °C with constant agitation to generate preformed Aβ aggregates. The resulting samples were then treated with compounds (50 μM) and incubated with constant agitation for additional 24 h.

3.4.9. Gel electrophoresis and Western blotting

The samples from the inhibition and disaggregation experiments were analyzed by gel electrophoresis followed by Western blotting using an anti-Aβ antibody (6E10) using previously established procedures.[14,18,32,33,56,60,61] Samples (10 μL) were separated on a 10-20% Tris-tricine gel (Invitrogen, Grand Island, NY, USA). Following separation, the proteins were transferred onto nitrocellulose membranes and blocked with bovine serum albumin (BSA, 3% w/v, Sigma-Aldrich, St. Louis, MO, USA) in Tris-buffered saline (TBS) containing 0.1% Tween-20 (TBS-T) for 2 h at room temperature or overnight at 4 °C. The membranes were incubated with an anti-Aβ antibody (6E10, 1:2000, Covance, Princeton, NJ, USA) in a solution of 2% BSA (w/v in TBS-T) for 4 h at room temperature or overnight at 4 °C. After washing with TBS-T (3x, 10 min), a horseradish peroxidase-conjugated goat antimouse secondary antibody (1:5000 in 2% BSA w/v in TBS-T; Cayman Chemical Company, Ann Arbor, MI, USA) was added for 1 h at room temperature. The ThermoScientific SuperSignal West Pico Chemiluminescent Substrate (Thermo Scientific, Rockford, IL, USA), Biosesang ECL Plus kit (Biosesang,

Gyeonggi-do, Republic of Korea), or a homemade ECL kit[62] was used to visualize the results on a ChemiDoc MP Imaging System (Bio-Rad, Hercules, CA, USA) or film.

3.4.10. Transmission electron microscopy (TEM)

Samples for TEM were prepared according to a previously reported method using glow-discharged grids (Formar/Carbon 300-mesh, Electron Microscopy Sciences, Hatfield, PA, USA).[14,18,32,33,56,60,61] Images for each sample were taken on a JEOL JEM-2100 transmission electron microscope (UNIST Central Research Facilities, Ulsan National Institute of Science and Technology, Ulsan, Republic of Korea).

3.5.11. Cell viability studies

The human neuroblastoma M17 cell line was purchased from the American Type Culture Collection (ATCC, Manassas, VA, USA). The cell line was maintained in media containing 50% minimum essential medium (MEM) and 50% F12 (GIBCO, Grand Island, NY, USA), supplemented with 10% fetal bovine serum (FBS, Sigma), 100 U/mL penicillin, and 100 mg/mL streptomycin (GIBCO). The cells were grown and maintained at 37 °C in a humidified atmosphere with 5% CO_2. Cell viability upon treatment of compounds was determined using the MTT assay (Sigma). M17 cells were seeded in a 96 well plate (15,000 cells in 100 μL per well). The cells were treated with Aβ (20 μM) with or without $CuCl_2$ or $ZnCl_2$ (20 μM), followed by the addition of compound (20 μM, 1% v/v final DMSO concentration) and incubated for 24 h with the cells. After incubation, 25 μL MTT (5 mg/mL in phosphate buffered saline (PBS, pH 7.4, GIBCO) was added to each well and the plate was incubated for 4 h at 37 °C. Formazan produced by the cells was solubilized using an acidic solution of *N*,*N*-dimethylformamide (DMF, 50%, v/v aq) and sodium dodecyl sulfate (SDS, 20%, w/v) overnight at room temperature in the dark. The absorbance was measured at 600 nm using a microplate reader. Cell viability was calculated relative to cells containing an equivalent amount of DMSO.

3.4.12. Primary neuron cultures

Mouse primary neuron cultures where prepared from embryonic day 17-18 (E17-

18) embryos harvested from pregnant C57BL/6 mice. The mice were reared and housed in accordance with the University of Michigan's Unit for Laboratory Animal Medicine (ULAM) guidelines for humane treatment of research animals. All protocols employed received prior approval from University of Michigan's University Committee on the Use and Care of Animals (UCUCA). The brains were excised in Hank's balanced salt solution (HBSS) supplemented with antibiotic-antimycotic (anti-anti) and 2 mM L-glutamine (gln) (Gibco). Prefrontal cortices where dissected, minced, tryptinized (Gibco) and triturated in G2 medium (neurobasal, B27 supplement, gln, anti-anti, all Gibco). Three hundred thousand cells were plated onto a ∅18 mm round coverslip (Deutsche Spiegelglas, Carolina Biological Supply Company) that was acid-treated and coated with poly-D-lysine (PDL, Sigma) and placed in a well of a 12-well plate. Alternatively, cells were added directly into G2 media within PDL-treated plastic wells. Cultures were maintained in a humidified atmosphere at 37 °C and 5% CO_2. A regular feeding schedule was maintained over 21 days *in vitro* (DIV). Compound stocks were formulated in DMSO and diluted in G2 media. Neurons at 21 DIV were treated to a range of compound concentrations at 0, 10, 40 and 100 μM. The final DMSO concentration never exceeded 1%, which did not affect neuron viability within experimental error. Neuron viability was assayed using the MTT assay following *ca*. 72 h culture incubation with compound. MTT (5 mg/mL, Sigma) was added and samples were maintained an additional 4 h at 37 °C to allow viable cells time to metabolize the MTT to formazan. After 4 h, the media was aspirated, and a formazan solubilizing solution (20% SDS in 1:1 dimethyl formamide:H_2O) was added and left overnight. Absorbance at 600 nm was recorded the following day. In parallel, controls of compound in G2 media devoid of neuron culture were also prepared to rule out the possibility that the compounds might interfere with the MTT assay.

3.4.13. Antioxidant assay

The antioxidant activity of **1**-**4** was determined by the TEAC assay employing N2a cell line (ATCC) lysates following the previous reported procedures.[18,33,34,60]

3.4.14. 2-Deoxyribose assay

The ability of **1**-**3** to decrease free radical formation from Fenton-like chemistry by Cu(I/II) was determined using previously reported procedures.[33,34] To summarize, chelexed solutions of phosphate buffer (50 mM, NaH_2PO_4, pH 7.2), compound (125 μM in water), $CuCl_2$ (10 μM), 2-deoxy-D-ribose (15 mM), H_2O_2 (200 μM), and sodium ascorbate (2 mM) were mixed in the listed order and incubated at 37 °C with constant agitation. After 1 h, the samples were quenched with trichloroacetic acid (2.8% w/v, 200 μL) and 2-thiobarbituric acid (1% w/v, 200 μL) and heated at 100 °C for 20 min. The samples were allowed to cool for 5 min before measuring the absorbance values at 532 nm on a microplate reader. Samples without compound were also tested as a control. Normalized absorbance values were calculated as previously reported.[33]

3.4.15. Determination of solution speciation for 1, 2, 3, and Cu(II)–3 complex

The pK_a values for **1-3** were determined by UV−Vis variable-pH titrations as previously reported.[14,56,61,63-66] To establish the pK_a values, a solution (100 mM NaCl, 10 mM NaOH, pH 12) of **1** (50 μM), **2** (20 μM), or **3** (100 μM) was titrated with small amounts of HCl. At least 30 spectra were recorded in the range of pH 2−10. Similarly, a solution containing $CuCl_2$ and **3** (50 μM) in a metal to ligand ratio of 1:2 was titrated with small additions of HCl and at least 30 spectra were recorded over the range pH 2−7. The acidity and stability constants were calculated by using the HypSpec program (Protonic Software, UK).[67] Speciation diagrams were modeled in the HySS2009 program (Protonic Software).[68]

3.4.16. Stability studies

The stability of **1**-**4** (50 μM) in the absence and presence of $CuCl_2$ (25 μM) were monitored every 10 min using UV-Vis spectroscopy for 5 h in buffer (20 μM HEPES, 150 μM NaCl, 1% DMSO, pH 7.4) at 37 ^{o}C. The resulting spectra were corrected for baseline shifts at 800 nm and the half-life and rate of decay of the absorbance at 250, 385, and 400 nm for **4**, [Cu(II) + **1**], and [Cu(II) + **2**], respectively**,** was calculated using the first order exponential decay function as implemented in Origin 9.1 (OrginLab Corp., Northampton, MA, USA). Additionally, the species present were identified using ESI(+)MS on a Bruker HCT basic system mass spectrometer equipped with an ESI ion

source. Triplicate samples determined the mass accuracy of the instrument to be approximately ±1 Da. Samples containing **1**-**4** (50 μM) with or without $CuCl_2$ (25 μM) were incubated in ddH_2O (1% DMSO) at 37 °C for the selected time points before being flash frozen using liquid nitrogen and stored at −80 °C until thawed immediately before measurement.

3.4.17. Calculation of transition state energies and ionization potentials

First-principles calculations using Gaussian09[69] were carried out for **1**-**4** in order to study the S_N2 hydrolysis and their one and two electron oxidation. For the direct C–N bond hydrolysis mechanism assisted by Cu(II), five additional water molecules were added to the first hydration sphere of Cu(II) in addition to the water molecule acting as a nucleophile. The structure optimizations were performed in the vacuum at M06/6-31G(d) level. The Los Alamos effective-core potential (ECP) LanL2DZ basis set was applied for Cu(II). The hydration effect was taken into account by additional single point calculations with polarizable continuum model (PCM) at M06/6-31G(d) level. The M06 exchange−correlation functional was chosen over other more commonly used functionals such as B3LYP due to calculated values using M06 in test datasets for similar calculations better match experimental values.[70,71] To find transition states as the first-order saddle points on the PES, Berny algorithm was used. The validity of the transition states were confirmed by frequency calculations (one imaginary) corresponding to the translational motion of the carbon from C–N bond. For the oxidation of **1**-**4**, we assumed one electron oxidations and two electron oxidations with subsequent proton loss and calculated only thermodynamic parameters due to the difficulty of computing the kinetics of electron transfer steps. All the relevant chemical species were optimized at M06/6-31G(d) level, and their thermodynamic parameters were calculated at M06/6-311+G(2df,2p) level.

3.5. Acknowledgements

This work was supported by the Research Fund (Project Number 1.140101.01) of Ulsan National Institute of Science and Technology (UNIST) (to M.H.L.); the University of Michigan Protein Folding Disease Initiative (to B.Y., B.T.R., and M.H.L.).

3.6. References

(1) Bush, A. I. *Curr. Opin. Chem. Biol.* **2000**, *4*, 184.
(2) Beck, M. W.; Pithadia, A. S.; DeToma, A. S.; Korshavn, K. J.; Lim, M. H. In *Ligand Design in Medicinal Inorganic Chemistry*; Storr, T., Ed. Wiley: Chichester, **2014**; pp. 256.
(3) Leal, S. S.; Botelho, H. M.; Gomes, C. M. *Coord. Chem. Rev.* **2012**, *256*, 2253.
(4) Viles, J. H. *Coord. Chem. Rev.* **2012**, *256*, 2271.
(5) Rivera-Mancía, S.; Pérez-Neri, I.; Ríos, C.; Tristán-López, L.; Rivera-Espinosa, L.; Montes, S. *Chem. Biol. Interact.* **2010**, *186*, 184.
(6) Emerit, J.; Edeas, M.; Bricaire, F. *Biomed. Pharmacother.* **2004**, *58*, 39.
(7) Soto, C. *Nat. Rev. Neurosci.* **2003**, *4*, 49.
(8) Rowinska-Zyrek, M.; Salerno, M.; Kozlowski, H. *Coord. Chem. Rev.* **2015**, *284*, 298.
(9) Kepp, K. P. *Chem. Rev.* **2012**, *112*, 5193.
(10) Savelieff, M. G.; Lee, S.; Liu, Y.; Lim, M. H. *ACS Chem. Biol.* **2013**, *8*, 856.
(11) Greenough, M. A.; Camakaris, J.; Bush, A. I. *Neurochem. Int.* **2013**, *62*, 540.
(12) Faller, P.; Hureau, C. *Eur. J. Chem.* **2012**, *18*, 15910.
(13) Rodríguez-Rodríguez, C.; Telpoukhovskaia, M.; Orvig, C. *Coord. Chem. Rev.* **2012**, *256*, 2308.
(14) Choi, J.-S.; Braymer, J. J.; Nanga, R. P. R.; Ramamoorthy, A.; Lim, M. H. *Proc. Natl. Acad. Sci. USA* **2010**, *107*, 21990.
(15) Kung, H. F.; Lee, C.-W.; Zhuang, Z.-P.; Kung, M.-P.; Hou, C.; Plössl, K. *J. Am. Chem. Soc.* **2001**, *123*, 12740.
(16) Cary, B. P.; Brooks, A. F.; Fawaz, M. V.; Shao, X.; Desmond, T. J.; Carpenter, G. M.; Sherman, P.; Quesada, C. A.; Albin, R. L.; Scott, P. J. H. *ACS Med. Chem. Lett.* **2014**, *6*, 112.
(17) Hindo, S. S.; Mancino, A. M.; Braymer, J. J.; Liu, Y.; Vivekanandan, S.; Ramamoorthy, A.; Lim, M. H. *J. Am. Chem. Soc.* **2009**, *131*, 16663.
(18) Beck, M. W.; Oh, S. B.; Kerr, R. A.; Lee, H. J.; Kim, S. H.; Jang, M.; Ruotolo, B. T.; Lee, J.-Y.; Lim, M. H. *Chem. Sci.* **2015**, *6*, 1879.
(19) Jones, C. K.; Engers, D. W.; Thompson, A. D.; Field, J. R.; Blobaum, A. L.; Lindsley, S. R.; Zhou, Y.; Gogliotti, R. D.; Jadhav, S.; Zamorano, R.; Bogenpohl, J.; Smith, Y.; Morrison, R.; Daniels, J. S.; Weaver, C. D.; Conn, P. J.; Lindsley, C. W.; Niswender, C. M.; Hopkins, C. R. *J. Med. Chem.* **2011**, *54*, 7639.
(20) Sharma, U.; Verma, P. K.; Kumar, N.; Kumar, V.; Bala, M.; Singh, B. *Chem. Eur. J.* **2011**, *17*, 5903.
(21) Kerns, E. H.; Di, L. In *Drug-like properties: concepts, structure design and methods*: from ADME to toxicity optimization; Kerns, E. H., Di, L., Eds.; Academic Press: San Diego, **2008**; pp 86.
(22) Barnham, K. J.; Masters, C. L.; Bush, A. I. *Nat. Rev. Drug Discov.* **2004**, *3*, 205.
(23) Ayton, S.; Lei, P.; Bush, A. I. *Free Radic. Biol. Med.* **2013**, *62*, 76.
(24) Pithadia, A. S.; Lim, M. H. *Curr. Opin. Chem. Biol.* **2012**, *16*, 67.
(25) Faller, P.; Hureau, C. *Dalton Trans.* **2009**, 1080.
(26) Faller, P.; Hureau, C.; La Penna, G. *Acc. Chem. Res.* **2014**, *47*, 2252.
(27) Lee, H. J.; Korshavn, K. J.; Kochi, A.; Derrick, J. S.; Lim, M. H. *Chem. Soc. Rev.* **2014**, *43*, 6672.

(28) DeToma, A. S.; Salamekh, S.; Ramamoorthy, A.; Lim, M. H. *Chem. Soc. Rev.* **2012**, *41*, 608.
(29) Savelieff, M. G.; DeToma, A. S.; Derrick, J. S.; Lim, M. H. *Acc. Chem. Res.* **2014**, *47*, 2475.
(30) Telpoukhovskaia, M. A.; Orvig, C. *Chem. Soc. Rev.* **2013**, *42*, 1836.
(31) Rauk, A. *Chem. Soc. Rev.* **2009**, *38*, 2698.
(32) Hyung, S.-J.; DeToma, A. S.; Brender, J. R.; Lee, S.; Vivekanandan, S.; Kochi, A.; Choi, J.-S.; Ramamoorthy, A.; Ruotolo, B. T.; Lim, M. H. *Proc. Natl. Acad. Sci. USA* **2013**, *110*, 3743.
(33) Lee, S.; Zheng, X.; Krishnamoorthy, J.; Savelieff, M. G.; Park, H. M.; Brender, J. R.; Kim, J. H.; Derrick, J. S.; Kochi, A.; Lee, H. J.; Kim, C.; Ramamoorthy, A.; Bowers, M. T.; Lim, M. H. *J. Am. Chem. Soc.* **2014**, *136*, 299.
(34) Charkoudian, L. K.; Pham, D. M.; Franz, K. J. *J. Am. Chem. Soc.* **2006**, *128*, 12424.
(35) Nam, Y. *et al.* **2015** Unpublished Results.
(36) Potts, H. A.; Smith, G. F. *J. Chem. Soc.* **1957**, 4018.
(37) Tan, Y.; Ghandi, K. *Synth. Met.* **2013**, *175*, 183.
(38) Michaelis, L.; Schubert, M. P.; Granick, S. *J. Am. Chem. Soc.* **1939**, *61*, 1981.
(39) Esmaili, R.; Nematollahi, D. *Electrochim. Acta* **2011**, *56*, 3899.
(40) Esmaili, R.; Varmaghani, F.; Nematollahi, D. *J. Electrochem. Soc.* **2012**, *159*, H680.
(41) Compton, R. G.; King, P. M.; Reynolds, C. A.; Richards, W. G.; Waller, A. M. *J. Electroanal. Chem. Interfacial Electrochem.* **1989**, *258*, 79.
(42) Ito, A.; Sakamaki, D.; Ino, H.; Taniguchi, A.; Hirao, Y.; Tanaka, K.; Kanemoto, K.; Kato, T. *Eur. J. Org. Chem.* **2009**, *2009*, 4441.
(43) Maleki, A.; Nematollahi, D. *J. Electroanal. Chem.* **2013**, *704*, 75.
(44) Modestov, A. D.; Gun, J.; Savotine, I.; Lev, O. *J. Electroanal. Chem.* **2004**, *565*, 7.
(45) Banks, C. E.; Lawrence, N. S.; Compton, R. G. *Electroanalysis* **2003**, *15*, 243.
(46) Nickel, U.; Peris, C. V.; Ramminger, U. *J. Phys. Chem. A* **2002**, *106*, 3773.
(47) Guilloreau, L.; Damian, L.; Coppel, Y.; Mazarguil, H.; Winterhalter, M.; Faller, P. *J. Biol. Inorg. Chem.* **2006**, *11*, 1024.
(48) Hureau, C.; Dorlet, P. *Coord. Chem. Rev.* **2012**, *256*, 2175.
(49) Swinehart, D. F. *J. Chem. Educ.* **1962**, *39*, 333.
(50) Hawkins, C.; Davies, M. J. *BBA-Bioenergetics* **2001**, *1504*, 196.
(51) Garrison, W. M. *Chem. Rev.* **1987**, *87*, 381.
(52) Porter, M. R.; Kochi, A.; Karty, J. A.; Lim, M. H.; Zaleski, J. M. *Chem. Sci.* **2014**, *6*, 1018.
(53) Davies, M. J. *Arch. Biochem. Biophys.* **1996**, *336*, 163.
(54) Lü, J.-M.; Lin, P. H.; Yao, Q.; Chen, C. *J. Cell. Mol. Med.* **2010**, *14*, 840.
(55) Halliwell, B. *Adv. Pharmacol.* **1996**, *38*, 3.
(56) Pithadia, A. S.; Kochi, A.; Soper, M. T.; Beck, M. W.; Liu, Y.; Lee, S.; DeToma, A. S.; Ruotolo, B. T.; Lim, M. H. *Inorg. Chem.* **2012**, *51*, 12959.
(57) Di, L.; Kerns, E. H.; Fan, K.; McConnell, O. J.; Carter, G. T. *Eur. J. Med. Chem.* **2003**, *38*, 223.

(58) Avdeef, A.; Bendels, S.; Di, L.; Faller, B.; Kansy, M.; Sugano, K.; Yamauchi, Y. *J. Pharm. Sci.* **2007**, *96*, 2893.
(59) *BBB Protocol and Test Compounds*; pION Inc.: Woburn, MA, 2009.
(60) Savelieff, M. G.; Liu, Y.; Senthamarai, R. R. P.; Korshavn, K. J.; Lee, H. J.; Ramamoorthy, A.; Lim, M. H. *Chem. Commun.* **2014**, *50*, 5301.
(61) Liu, Y.; Kochi, A.; Pithadia, A. S.; Lee, S.; Nam, Y.; Beck, M. W.; He, X.; Lee, D.; Lim, M. H. *Inorg. Chem.* **2013**, *52*, 8121.
(62) Mruk, D. D.; Cheng, C. Y. *Spermatogenesis* **2011**, *1*, 121.
(63) Choi, J.-S.; Braymer, J. J.; Park, S. K.; Mustafa, S.; Chae, J.; Lim, M. H. *Metallomics* **2011**, *3*, 284.
(64) Braymer, J. J.; Choi, J.-S.; DeToma, A. S.; Wang, C.; Nam, K.; Kampf, J. W.; Ramamoorthy, A.; Lim, M. H. *Inorg. Chem.* **2011**, *50*, 10724.
(65) He, X.; Park, H. M.; Hyung, S.-J.; DeToma, A. S.; Kim, C.; Ruotolo, B. T.; Lim, M. H. *Dalton Trans.* **2012**, *41*, 6558.
(66) Braymer, J. J.; Merrill, N. M.; Lim, M. H. *Inorg. Chim. Acta* **2012**, *380*, 261.
(67) Gans, P.; Sabatini, A.; Vacca, A. *Ann. Chim.* **1999**, *89*, 45.
(68) Alderighi, L.; Gans, P.; Ienco, A.; Peters, D.; Sabatini, A.; Vacca, A. *Coord. Chem. Rev.* **1999**, *184*, 311.
(69) Gaussian 09, Revision **A.02**, Frisch, M. J.; Trucks, G. W.; Schlegel, H. B.; Scuseria, G. E.; Robb, M. A.; Cheeseman, J. R.; Scalmani, G.; Barone, V.; Mennucci, B.; Petersson, G. A.; Nakatsuji, H.; Caricato, M.; Li, X.; Hratchian, H. P.; Izmaylov, A. F.; Bloino, J.; Zheng, G.; Sonnenberg, J. L.; Hada, M.; Ehara, M.; Toyota, K.; Fukuda, R.; Hasegawa, J.; Ishida, M.; Nakajima, T.; Honda, Y.; Kitao, O.; Nakai, H.; Vreven, T.; Montgomery, J. A., Jr.; Peralta, J. E.; Ogliaro, F.; Bearpark, M.; Heyd, J. J.; Brothers, E.; Kudin, K. N.; Staroverov, V. N.; Kobayashi, R.; Normand, J.; Raghavachari, K.; Rendell, A.; Burant, J. C.; Iyengar, S. S.; Tomasi, J.; Cossi, M.; Rega, N.; Millam, M. J.; Klene, M.; Knox, J. E.; Cross, J. B.; Bakken, V.; Adamo, C.; Jaramillo, J.; Gomperts, R.; Stratmann, R. E.; Yazyev, O.; Austin, A. J.; Cammi, R.; Pomelli, C.; Ochterski, J. W.; Martin, R. L.; Morokuma, K.; Zakrzewski, V. G.; Voth, G. A.; Salvador, P.; Dannenberg, J. J.; Dapprich, S.; Daniels, A. D.; Farkas, Ö.; Foresman, J. B.; Ortiz, J. V.; Cioslowski, J.; Fox, D. J. Gaussian, Inc., Wallingford CT, **2009**.
(70) Zhao, Y.; Truhlar, D. G. *Acc. Chem. Res.* **2008**, *41*, 157.
(71) Zhao, Y.; Truhlar, D. G. *Theor. Chem. Acc.* **2007**, *120*, 2.

Chapter 4
Utilizing divergent pathways of activities to mediate multiple features in Alzheimer's disease

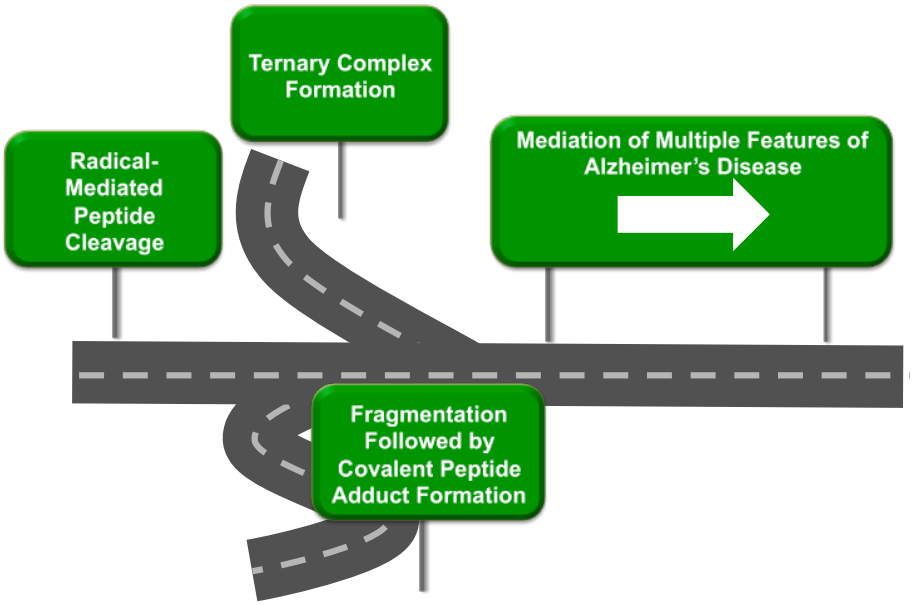

I thank Professor Ayyalusamy Ramamoorthy and Kyle Korshavn for NMR studies as well as Professor Kwang Soo Kim, Dr. Han Lee, Dr. Woo Cho, and Dr. Zahra Tehrani for computational calculations. I also appreciate Professor Scott Larsen's assistance in designing the compounds. Younwoo Nam obtained the TEM images. Milim Jang performed the cytotoxicity studies and antioxidant capacity assay. I performed the gel/Western blot, inhibition of Fenton chemistry, the PAMPA-BBB permeability assay, and mechanistic studies in solution experiments.

4.1. Introduction

Effective diagnostic tools and treatments for neurodegenerative diseases have been unavailable to date due to multiple reasons. One reason is the lack of understanding of the underlying pathogenesis required in order to develop such medical interventions.[1-7] This is highlighted in Alzheimer's disease (AD) where, despite being one of the better-studied neurodegenerative diseases, the etiology is still unclear.[1-5,7-9] The current understanding of AD implicates multiple factors that could be interrelated.[1-3,5,7,10-15] Recently, an area of particularly high interest is the interrelationship between the observed metal ion dyshomeostasis, abnormal aggregation and accumulation of the intrinsically disordered protein (IDP) amyloid-β (Aβ), and increased oxidative stress in the brain. Metal ions have been suggested to be central to this interrelationship as several biologically relevant metal ions [*e.g.*, Fe(II/III), Cu(I/II), and Zn(II)] have been shown *in vitro* to bind to Aβ.[1-3,5,10-14,16] Additionally, the coordination of Aβ to redox active metal ions [Fe(II/III), Cu(I/II)] has been shown to facilitate the production of reactive oxygen species (ROS) through Fenton-like chemistry.[1-3,5,10-12,14,17-20]

In order to elucidate this interrelationship in depth, chemical tools have been developed to target these interrelated factors and mediate their reactivities. The molecular-level modes of action of many of these tools, however, are not well studied.[1,2,21] This limits the ability to make rational optimization to their structures to improve their activity. Recently, we have reported the development of some small molecules (**1**-**4**) which have different modes of action, despite being structurally similar, for targeting and reducing the aggregation of metal-free Aβ and metal–Aβ as well as the formation of ROS (reactivity) overall diminishing toxicity (Figure 4.1).[22] These initial studies with **1**-**4** resulted in the proposal of three possible structure-dependent mechanisms for their differing activities (Figure 4.2): (a) The generation of a transient ternary complex with Cu(II)–Aβ followed by the one electron oxidation of the compounds producing a radical which results in cleavage of the Aβ peptide in the first five residues (**1** and **2**); (b) the formation of a stable ternary complex with metal–Aβ (**3**); (c) the hydrolysis of the compound to generate dimethyl-4-phenylenediamine (**DMPD**) which is a molecule known to interact with and mediate metal-free Aβ and metal–Aβ reactivity (**4**; Figure 4.2).[22]

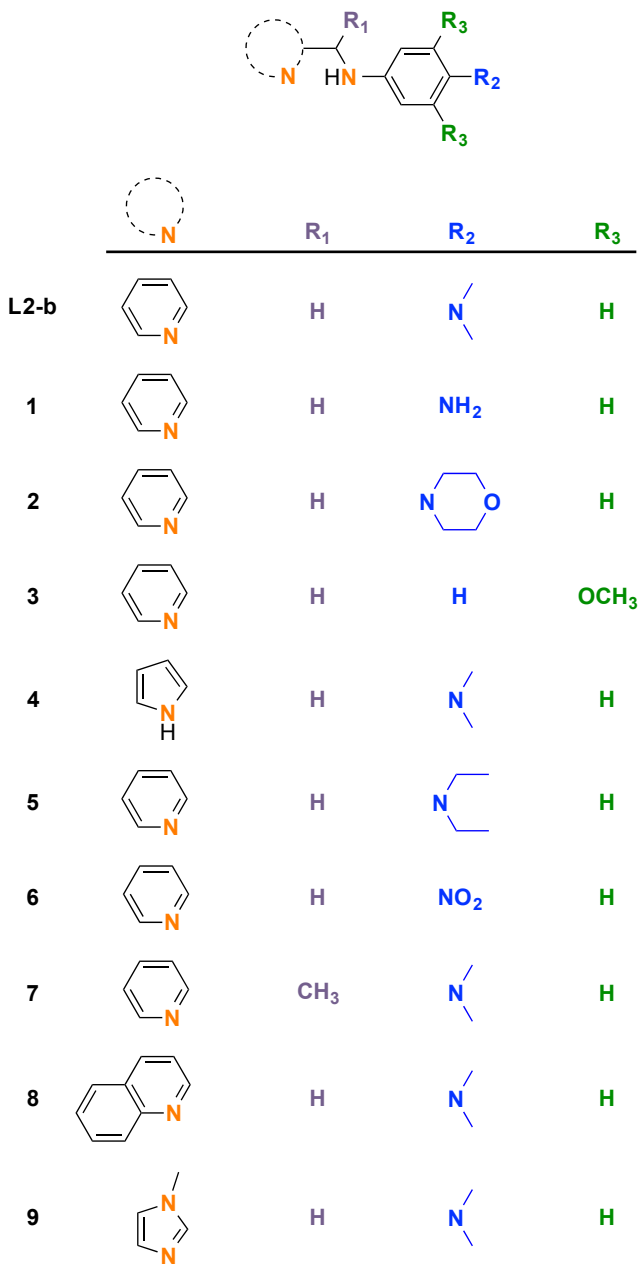

Figure 4.1. Structures of stilbene derivatives designed to target metal-free and metal-bound Aβ and modulate their reactivity. **L2-b** = N^1,N^1-Dimethyl-N^4-(pyridin-2-ylmethyl)benzene-1,4-diamine; **1** = N^1-(pyridin-2-ylmethyl)benzene-1,4-diamine; **2** = 4-morpholino-*N*-(pyridin-2-ylmethyl)aniline; **3** = 3,5-dimethoxy-*N*-(pyridin-2-ylmethyl)aniline; **4** = N^1-((1*H*-pyrrol-2-yl)methyl)-N^4,N^4-dimethylbenzene-1,4-diamine; **5** = N^1,N^1-diethyl-N^4-(pyridin-2-ylmethyl)benzene-1,4-diamine; **6** = 4-nitro-*N*-(pyridin-2-ylmethyl)aniline; **7** = N^1,N^1-dimethyl-N^4-(1-(pyridin-2-yl)ethyl)benzene-1,4-diamine; **8** = N^1,N^1-dimethyl-N^4-(quinolin-2-ylmethyl)benzene-1,4-diamine; **9** = N^1,N^1-dimethyl-N^4-((1-methyl-1*H*-imidazol-2-yl)methyl)benzene-1,4-diamine.

Herein, we report the rational design, the ability to control the mode of action and thus the reactivity of Aβ and metal–Aβ, as well as, the detailed, molecular-level characterization of a series of small molecules (**1**-**9,** Figure 4.1). Additionally, the mode

of action of **L2-b** (Figure 4.1), a structurally similar molecule, which can specifically mediate metal–Aβ reactivity over metal-free Aβ *in vitro and in vivo* resulting in alleviated AD pathology and symptoms, is also studied.[22,23] Through chemical, biochemical, biophysical, and computational studies, we demonstrate that **5**-**9** and **L2-b** like **1**-**4** have structure-dependent capabilities to modulate the reactivity of metal-free Aβ and metal–Aβ. Detailed mode of action studies reveal that compounds that were more difficult to oxidize (**3** and **6**) had more limited abilities to control the reactivity of Aβ in the presence and absence of metal ions, while those that undergo oxidation more easily suppressed Cu(II)–Aβ reactivity but not that of metal-free Aβ (**1**, **2**, **5**, **7**-**9**, and **L2-b**). Activity toward Zn(II)–Aβ was proposed to be dependent on the ability of the compound to compete with Aβ for Zn(II) binding to most likely allow for the formation of a ligand–Zn(II)–Aβ ternary complex (**5**, **7**-**9**, and **L2-b**). The broad activity of **4** towards both metal-free Aβ and metal–Aβ reactivity was found to be dependent on its degradation to a known Aβ reactivity modulator. Together the studies presented here generate an understanding of the molecular level interactions of a chemical library of small molecules with targeted abilities to mediate specific pathogenic features of neurodegenerative diseases and provide design principles that could be applied to generate new molecules with similar abilities in the future in order to study or to treat these diseases.

4.2. Results and discussion

(a) Radical-Mediated Peptide Cleavage:

$$\mathbf{L} + Cu(II)_n\text{–}A\beta \longrightarrow [\mathbf{L}\text{–}Cu(II)_n\text{–}A\beta] \longrightarrow [\mathbf{L}^{+\bullet}\text{–}Cu(I)_n\text{–}A\beta] \longrightarrow \mathbf{L}^{+} + Cu(I)_n + A\beta_{Degraded}$$

(b) Ternary Complex Formation:

$$\mathbf{L} + M(II)_n\text{–}A\beta \longrightarrow [\mathbf{L}\text{–}M(II)_n\text{–}A\beta]$$

(c) Fragmentation Followed by Covalent Peptide Adduct Formation

$$\mathbf{L} + H_2O \longrightarrow \mathbf{L}_{Fragment} + DMPD + A\beta \longrightarrow \mathbf{L}_{Fragment} + DMPD_{Transformed}\text{–}A\beta$$

Figure 4.2. Proposed mechanisms for reactivity of **1**-**9** with Aβ or metal–Aβ. (a) Ligand (**L**) forms a transient ternary complex with Cu(II)–Aβ. The Cu(II) oxidizes **L** to form the cationic radical of the ligand ($\mathbf{L}^{+\bullet}$) and the radical is transferred to Aβ resulting in the observed degradation of the peptide through radical-mediated cleavage. (b) **L** forms a stable ternary complex with metal–Aβ (M = Cu or Zn) resulting in the formation of a stable complex that redirects the aggregation of metal–Aβ reducing toxicity and oxidative stress. (c) Hydrolysis of **L**, which can be promoted by metal ions, produces a small molecule, **DMPD**, which has been show to covalently bind to Aβ controlling its reactivity.

4.2.1. Design principles for a chemical library

To generate a library of compounds able to interact with and modulate the aggregation of metal-free Aβ and metal–Aβ resulting in the formation of less toxic forms and reduce oxidative stress, the mechanistic insights into the activity of **1**-**4** from our initial studies[22] were utilized to modify the well-known amyloid-interacting stilbene framework (Figure 4.1).[23-27] In our initial studies, the electron donating properties of the aniline (in **1**) and 4-phenylmorpholine (in **2**) groups were suggested to be important in the formation of their radical forms required for activity.[22] Thus, new compounds, **5**, **7, 8**, and **9**, were constructed to contain electron-donating amine groups to allow for oxidation. **L2-b** also has an electron donating dimethylamino group. Additionally, a diethylamine group was installed in **5**, which is more electron donating than the dimethylamino components of **7**-**9** and **L2-b**. This is contrast to **6,** which has an electron withdrawing nitro moiety in order to reduce oxidation similar to the effect of the limited electron donating properties of 3,5-dimethoxybenzene moiety of **3** which does not oxidize in the presence of Cu(II).[22]

To confirm these design principles, density functional theory (DFT) calculations were performed to predict the one and two electron ionization potentials (IP_1 and IP_2, respectively) of these compounds as a measure of their ability to undergo oxidation (Table 4.1). As expected all compounds designed to undergo oxidation (**5**, **7**, **8**, and **9**) have similar or lower computed ionization potentials to the previously determined values for **1** and **2** (**1**, IP_1 = 6.23 eV, IP_2 = 6.02 eV; **2**, IP_1 = 6.06 eV, IP_2 = 6.02 eV) suggesting they will be able to produce the radical for believed to be necessary for activity (Table

Table 4.1. The first and second ionization potentials for **5**-**9** and **L2-b**.

Compound	IP_1 (eV)	IP_2 (eV)
5	5.82	5.91
6	7.75	8.16
7	6.01	5.83
8	5.90	6.13
9	6.10	6.06
L2-b	5.92	6.13

4.1).[22] Additionally, **L2-b** was calculated to be able to undergo oxidation having IP_1 and IP_2 values of 5.92 eV and 6.13 eV, respectively (Table 4.1). Moreover, as expected, the computational experiments showed that **5** could undergo oxidation more easily and that **6** was more difficult to oxidize than the other compounds (Table 4.1).

Furthermore, since the oxidation of these compounds is dependent on the binding of these compounds to Cu(II),[22] **7**-**9** were designed to modulate metal binding affinities to allow for more control of the activity of these compounds. The steric hindrance from the methyl group on the bridging carbon of **7** should cause the pyridyl nitrogen and the secondary amine to align to provide a metal binding site, enhancing metal binding. Based on hard-soft acid base (HSAB) theory, **8** with a quinoline group should have a slightly lower metal binding affinity than the compounds containing a pyridine moiety, while the methylimidazole moiety in **9** should effect a stronger metal binding affinity due to their relative Lewis basicities as reflected in their pK_a values.[28-30]

Table 4.2. Values (MW, *c*logP, HBA, HBD, PSA, logBB, and logP_e) of **5**-**9**.

Parameters	5	6	7	8	9	Lipinski's rules and Others
MW[a]	255	229	241	277	230	≤ 450
*c*LogP[b]	2.82	1.98	2.07	3.14	1.10	≤ 5.00
HBA[c]	3	5	3	3	4	≤ 10
HBD[d]	1	1	1	1	1	≤ 5
PSA (Å^2)[e]	28.2	76.2	28.2	28.2	33.1	≤ 90
logBB[f]	0.141	-0.696	0.0273	0.191	-0.193	< −1.0 poorly distributed in the brain
−logP_e[g]	4.4(2)	4.2(1)	4.3(7)	4.2(2)	4.7(3)	−logP_e < 5.4 (CNS+);
CNS +/− Prediction	CNS+	CNS+	CNS+	CNS+	CNS+	−logP_e > 5.7 (CNS-)

[a]MW, molecular weight; [b]*c*logP, calculated log of water–octanol partition coefficient; [c]HBA, hydrogen bond acceptor; [d]HBD, hydrogen bond donor; [e]PSA, polar surface area; [f]logBB = −0.0148 × PSA + 0.152 × *c*logP × 0.130; [g]Determined using the Parallel Artificial Membrane Permeability Assay adapted for BBB (PAMPA-BBB).

(a)

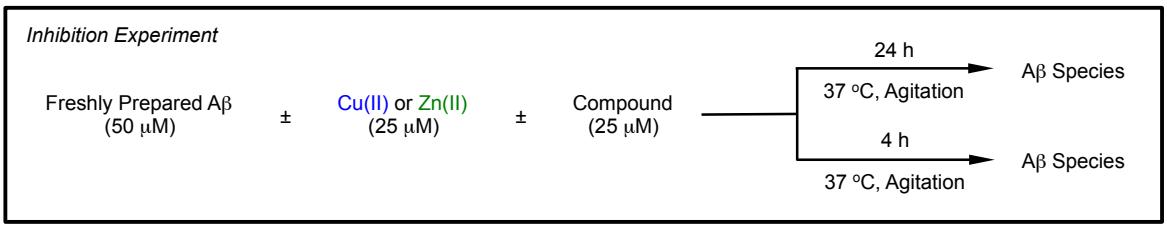
Inhibition Experiment
Freshly Prepared Aβ
(50 μM)
±
Cu(II) or Zn(II)
(25 μM)
±
Compound
(25 μM)
24 h
37 °C, Agitation
Aβ Species
4 h
37 °C, Agitation
Aβ Species

(a)

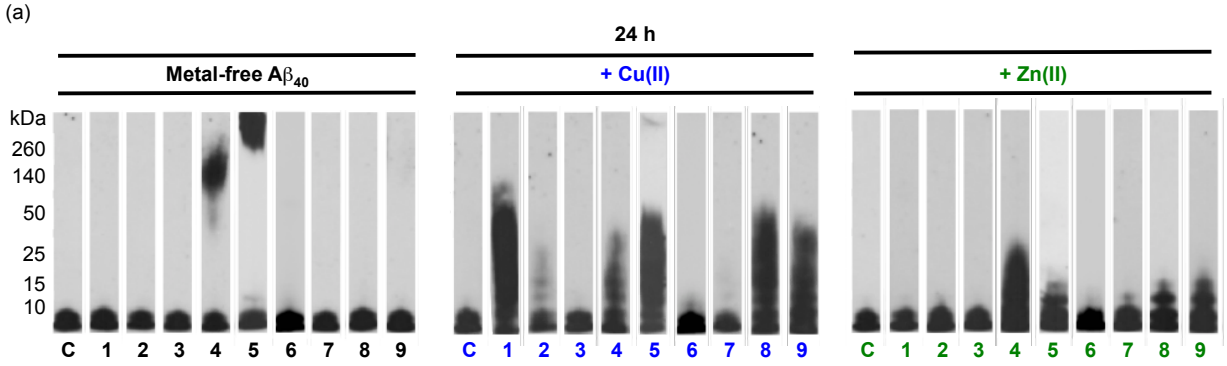
24 h
Metal-free Aβ40
+ Cu(II)
+ Zn(II)
kDa
260
140
50
25
15
10
C 1 2 3 4 5 6 7 8 9
C 1 2 3 4 5 6 7 8 9
C 1 2 3 4 5 6 7 8 9

(b)

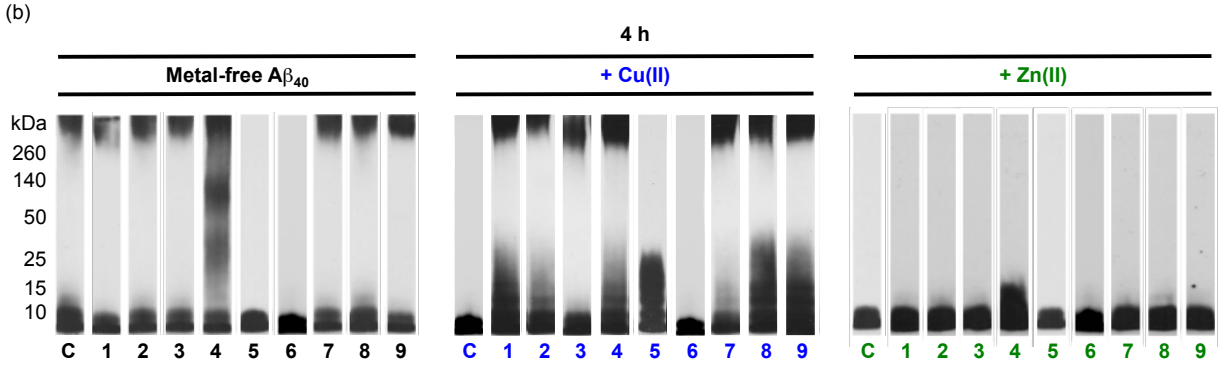
4 h
Metal-free Aβ40
+ Cu(II)
+ Zn(II)
kDa
260
140
50
25
15
10
C 1 2 3 4 5 6 7 8 9
C 1 2 3 4 5 6 7 8 9
C 1 2 3 4 5 6 7 8 9

(d)

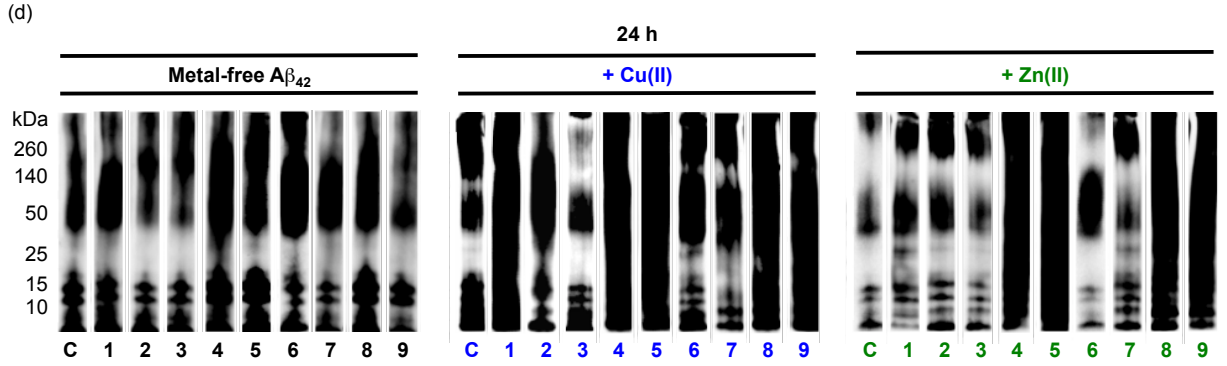
24 h
Metal-free Aβ42
+ Cu(II)
+ Zn(II)
kDa
260
140
50
25
15
10
C 1 2 3 4 5 6 7 8 9
C 1 2 3 4 5 6 7 8 9
C 1 2 3 4 5 6 7 8 9

(e)

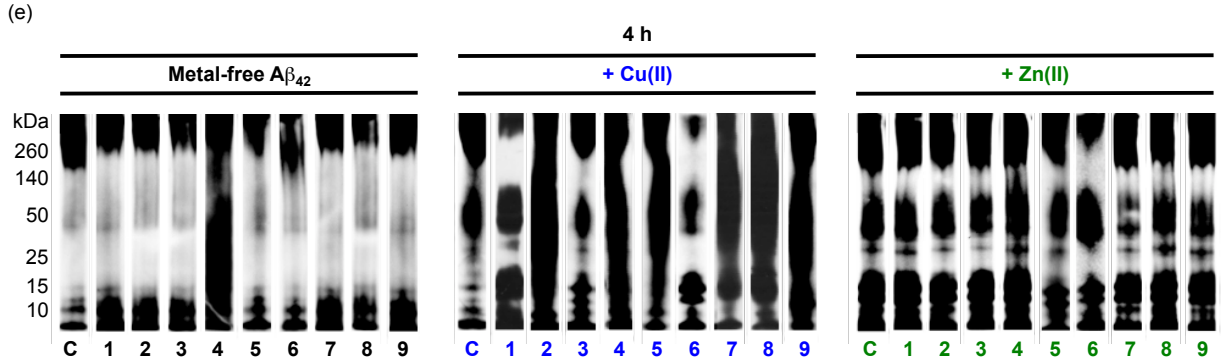
4 h
Metal-free Aβ42
+ Cu(II)
+ Zn(II)
kDa
260
140
50
25
15
10
C 1 2 3 4 5 6 7 8 9
C 1 2 3 4 5 6 7 8 9
C 1 2 3 4 5 6 7 8 9

Figure 4.3. Modulation of $A\beta_{40}$ and $A\beta_{42}$ aggregation by **1**-**9**. (a) Scheme of the inhibition experiment. Mixtures of freshly prepared Aβ with Cu(II) (blue), Zn(II) (green), or no metal ions were treated with compound (lanes 1-9) and incubated for 24 h or 4 h before analysis. Samples excluding compound (lane C) were also prepared as a control. Conditions: [Aβ] = 25 μM; [Cu(II) or Zn(II)] = 25 μM; [compound] = 50 μM; pH 6.6 (for Cu(II)-containing samples) or pH 7.4 (for metal-free and Zn(II)-containing samples); 37 ^{o}C; constant agitation. Analysis of the resulting molecular weights of (b, c) $A\beta_{40}$ and (d, e) $A\beta_{42}$ species after (b, d) 24 h or (c, e) 4 h incubation in the absence (left) or presence of Cu(II) (middle) or Zn(II) (right) by gel electrophoresis and subsequent Western blotting (gel/Western blot) with an anti-Aβ antibody (6E10).

The ability for these compounds to passively diffuse across the blood brain barrier (BBB) was also considered in the design by following Lipinski's rules and by using *in vitro* parallel artificial membrane permeability assay adapted for assessing BBB permeability (PAMPA-BBB) predicted that these compounds can passively diffuse across the BBB. The overall PAMPA-BBB results, along with calculated logBB values, suggest that these tools could be employed in the brain to target and modulate Aβ and metal–Aβ reactivity.

4.2.2. Modulation of metal-free Aβ and metal–Aβ aggregation

First, the ability of **1**-**9** to prevent Aβ aggregation (inhibition experiment; Figure 4.3a) and disassemble preformed Aβ aggregates (disaggregation experiment; Figure 4.4a) in the presence and absence of metal ions [Cu(II) and Zn(II)] were evaluated using gel electrophoresis followed by Western blot analysis (gel/Western blot) at short (4 h) and longer (24 h) time points. **1**-**4** were previously studied at the 24 h time point and are included to allow for comparison to the new studies at the 4 h interval.[22]

4 was found to be the only molecule capable of interacting with both metal– and metal-free Aβ (Figures 4.3b-e and 4.4b-e). In the case of metal-free Aβ, more noticeable changes were observed in the inhibition experiments at shorter time points and for $A\beta_{40}$ in the disaggregation experiments. Conversely, in the case of **5**, **8**, and **9,** the aggregation of Cu(II)–Aβ and Zn(II)–Aβ but not metal-free Aβ was redirected. Additionally, these compounds had a stronger effect at later time points with their activity toward Zn(II)–Aβ being negligible at early time points (Figures 4.3b-e and 4.4b-e). This is similar to the previously reported activity of **L2-b**.[22,24] **1**, **2**, **3**, and **7** could only modulate Cu(II)–Aβ aggregation and do so to different degrees (Figures 4.3b-e and 4.4b-e). **1** had a more noticeable affect at the longer time point while **2** had a stronger

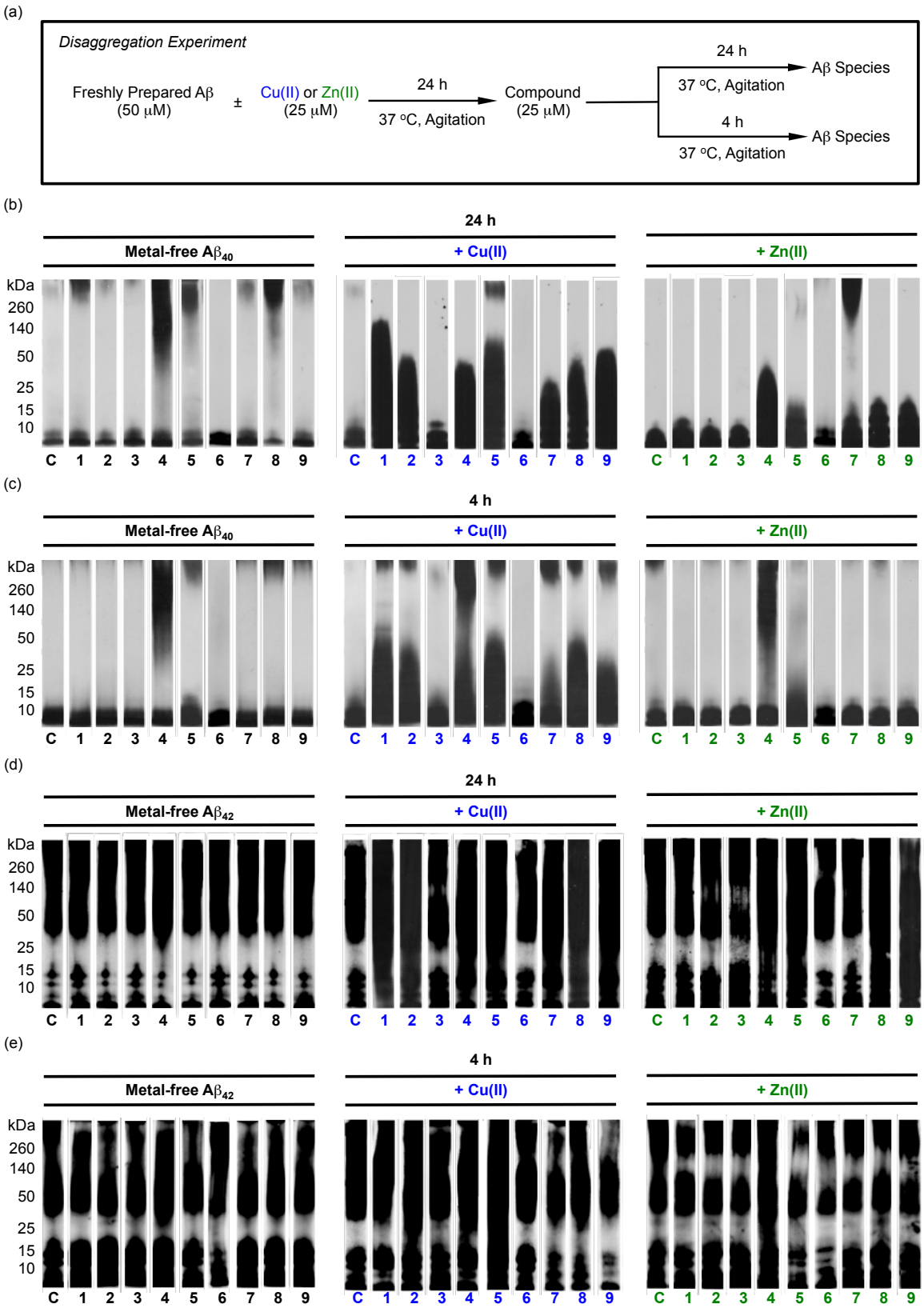

Figure 4.4. Disaggregation of preformed $A\beta_{40}$ and $A\beta_{42}$ aggregates by **1**-**9**. (a) Scheme of the inhibition

experiment. Mixtures of freshly prepared Aβ with Cu(II) (blue), Zn(II) (green), or no metal ions were treated with compound (lanes 1-9) and incubated for 24 h or 4 h before analysis. Samples excluding compound (lane C) were also prepared as a control. Conditions: [Aβ] = 25 μM; [Cu(II) or Zn(II)] = 25 μM; [compound] = 50 μM; pH 6.6 (for Cu(II)-containing samples) or pH 7.4 (for metal-free and Zn(II)-containing samples); 37 ^{o}C; constant agitation. Analysis of the resulting molecular weights of (b, c) $A\beta_{40}$ and (d, e) $A\beta_{42}$ species after (b, d) 24 h or (c, e) 4 h incubation in the absence (left) or presence of Cu(II) (middle) or Zn(II) (right) by gel electrophoresis and subsequent Western blotting (gel/Western blot) with an anti-Aβ antibody (6E10).

affect on aggregation at 4 h in both inhibition and disaggregation experiments (Figures 3b-e and 4.4b-e). **7** had the unique activity of being more prominent at earlier time points in the inhibition experiments but the opposite occurred in the disaggregation experiments where the ability to break up the preformed Cu(II)–Aβ aggregates was more clear at 24 h (Figures 3b-e and 4.4b-e). In both the inhibition and disaggregation experiments, **3** did not have a prominent effect on the aggregation of Cu(II)–Aβ under typical conditions; however, previous studies showed that **3** could control the aggregation of Cu(II)–Aβ at higher Cu(II) concentrations (Figures 4.3b-e and 4.4b-e).[22] **6** also did not have an apparent influence on Aβ aggregation; however, unlike **3** even at higher Cu(II) and Zn(II) concentrations no activity was observed (Figure 4.5).

Transmission electron microscopy (TEM) studies were carried out to visualize the morphology of Aβ aggregates after 24 h incubations with **5** and **7** (Figure 4.6). **5** did not have an impact on the type of the Aβ species in the absence of metal ions. In the presence of Cu(II) and Zn(II), however, **5** produced less structured, more amorphous Aβ aggregates. For **7**, TEM was only carried out on the Cu(II)–Aβ samples to help understand the differences in the varied reactivity in the inhibition and disaggregation experiments (*vide supra*). Despite showing limited activity in the gel/Western blot studies in the 24 h inhibition samples, long fibrils, which were indicated in the control samples, were not present after treatment with **7** (Figure 4.6a,c). This suggests that **7** could redirect the aggregation into larger species that cannot penetrate into the gels. While in disaggregation samples, where gel/Western blots showed activity, **7** produced shorter ($A\beta_{40}$) and thinner ($A\beta_{42}$) fibers (Figure 4.6b,d). As a whole, these experiments demonstrate that these compounds have different abilities to control metal-free and metal-induced Aβ aggregation.

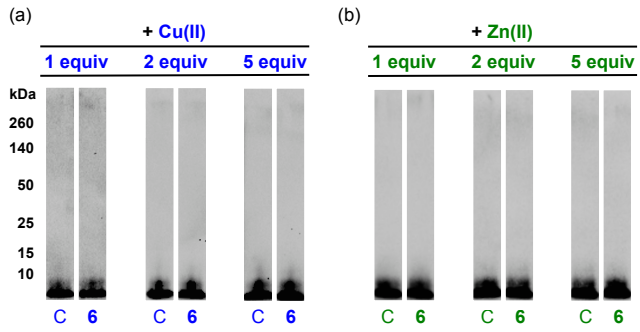

Figure 4.5. Inhibitory activity of compounds on $A\beta_{40}$ aggregation at higher ratios of metal to compound under the conditions of the inhibition experiments (Figure 4.3a). 1 equiv (left; 50 μM), 2 equiv (middle; 100 μM), and 5 equiv (right; 250 μM) of (a) Cu(II) and (b) Zn(II).

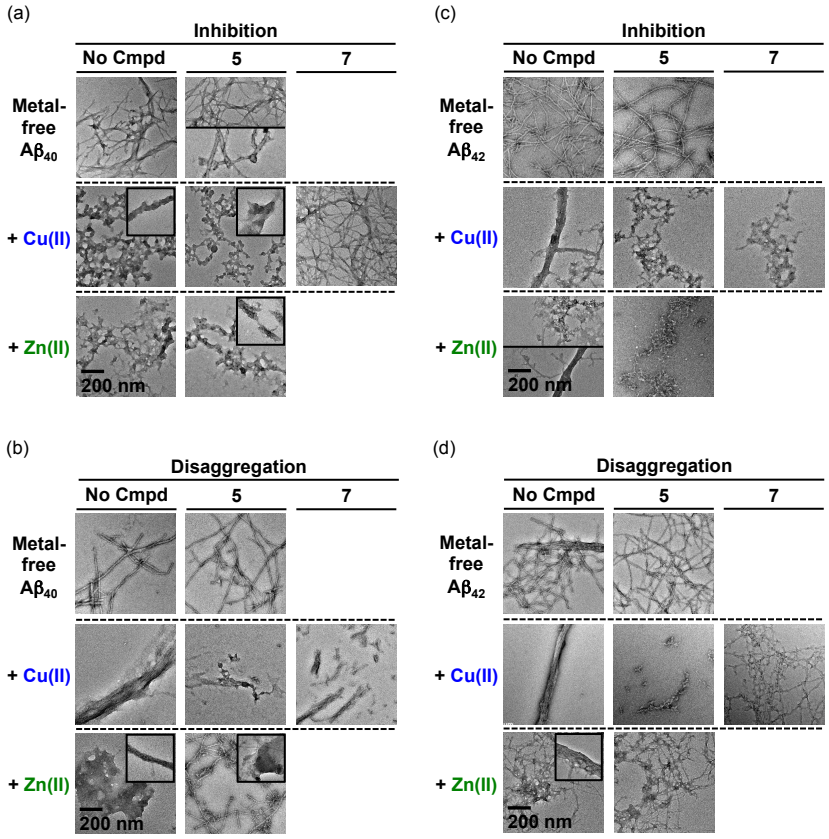

Figure 4.6. Morphologies of metal-free Aβ and metal–Aβ. TEM studies was employed to observe the morphologies of (a and b) $A\beta_{40}$ and (c and d) $A\beta_{42}$ from (a and c) inhibtion (Figure 4.3b and d) and (b and d) disaggregation experiments (Figure 4.4b and d) after 24 h incubation with **5** or **7**.

4.2.3. Proposed mode of action (I) for modulation of metal-free Aβ reactivity

In order to determine how **1**-**9** interact with and modulate metal-free Aβ aggregation, first, the species present in solution were studied. UV-Vis variable-pH